

**ROLE OF METAL SUPPORTED CATALYSTS AND THEIR  
CHARACTERIZATION IN THE CATALYTIC DECOMPOSITION OF  
METHANE FOR THE FORMATION OF UNIFORM CARBON  
NANOTUBES IN A SINGLE STEP PROCESS**

**CHAI SIANG PIAO**

**UNIVERSITI SAINS MALAYSIA  
2008**

**ROLE OF METAL SUPPORTED CATALYSTS AND THEIR  
CHARACTERIZATION IN THE CATALYTIC DECOMPOSITION OF  
METHANE FOR THE FORMATION OF UNIFORM CARBON  
NANOTUBES IN A SINGLE STEP PROCESS**

by

**CHAI SIANG PIAO**

**Thesis submitted in fulfillment of the requirements  
for the degree of  
Doctor of Philosophy**

**May 2008**

## ACKNOWLEDGEMENTS

My most sincere appreciation is forwarded to my main supervisor, Prof. Dr. Abdul Rahman Mohamed, for being an excellent mentor, taking precious time of his busy schedule to supervise my research activities and giving me expert guidance, constant attention, valuable comments and enthusiastic support throughout the whole course of this study. My heartfelt thanks also go to Dr. Sharif Hussein Sharif Zein, my co-supervisor, for providing constructive criticisms, invaluable discussions, incessant support, guidance and encouragement during my studies.

I would also like to thank Prof. Dr. Abdul Latif Ahmad, Dean of the School of Chemical Engineering USM, Dr. Syamsul Rizal Shukor and Dr. Mashitah Mat Don, Deputy Deans of the School of Chemical Engineering, for their continuous motivation, cultivated briefing on the postgraduate project requirements and invaluable help in postgraduate affairs throughout my studies. I would also like to extend my sincere appreciation to all lecturers in this school for giving me support and guidance, especially to Prof. Subhash Bhatia, Assoc. Prof. Dr. Bassim Hameed, Dr. Ahmad Zuhairi Abdullah, Dr. Lee Keat Teong and Dr. Tan Soon Huat, who have shared their precious knowledge of reaction engineering and catalysis with me.

I extend my gratitude to all the laboratory technicians and administrative staff of the School of Chemical Engineering USM, for the assistance rendered to me. A special acknowledgement also goes to the technicians from other schools in USM especially Mr. Pachamuthu and Mrs. Jamilah of the School of Biological Sciences for their warmhearted help in SEM and TEM analysis. To Mr. Karunakaran of the School of Physical Sciences and Mr. Kantasamy of the School of Chemical Sciences, their assistance in XRD and surface area analysis will always be remembered.

I also wish to record my sincere appreciation and thanks to former and current postgraduate students: Ali, Ahmed Mubarak, Ai Lien, Boon Seng, Cheng Teng, Choi Yee, Choe Peng, Derek, Fang Yin, Foo, Hossein, Irvan, Ivy, Jia Huey, Lau, Lian See, Mei Fong, Minoo, Pei Ching, Ramesh, Reza, Sam, Siew Chun, Sim Yee, Siva, Sunarti, Sumathi, Suzylawati, Thiam Leng, Wei Wen, Yean Sang, Yin Fong, Yen Thien and others whom I am not able to address here. Their invaluable discussions, support, patience and encouragement will be always remembered.

I am indeed very thankful to my dearest mother, Mdm. Khor Geok Hong, my brothers, Siang Teik and Siang Jen, my sisters-in-law, Sok Voon and Siew Ching, and finally to my loving girlfriend, Yar Ing. They are always on my side, riding along with me on my ups and downs as well as giving me encouragement to pursue my dreams. I also wish to dedicate this work in the memory of my beloved father, Mr. Chai Thian Fook, who passed away when I was in the midst of pursuing my studies. His enduring sacrifice to enable me to have a better future will be remembered forever.

Last but definitely not the least, I am very much indebted to the Ministry of Education and Universiti Sains Malaysia for providing me the financial support under Fundamental Research Grant Scheme (FRGS) (Project: A/C No: 6070014) and to the Academy Sciences of Malaysia for granting the Scientific Advancement Grant Allocation (SAGA) (Project A/C No: 6053001). I would also like to express my acknowledgement to the Ministry of Science, Technology and Innovations for providing me the postgraduate scholarship - Pasca Siswazah.

Thank you.

***CHAI SIANG PIAO***

***May 2008***

## TABLE OF CONTENTS

	Page
<b>ACKNOWLEDGEMENTS</b>	ii
<b>TABLE OF CONTENTS</b>	iv
<b>LIST OF TABLES</b>	viii
<b>LIST OF FIGURES</b>	xi
<b>LIST OF PLATES</b>	xix
<b>LIST OF ABBREVIATIONS</b>	xx
<b>LIST OF SYMBOLS</b>	xxii
<b>ABSTRAK</b>	xxiii
<b>ABSTRACT</b>	xxv
<b>CHAPTER 1 - INTRODUCTION</b>	1
1.1 Catalysis	1
1.2 Nanotechnology	2
1.3 Allotropes of Carbon	4
1.4 Carbon Nanotubes	5
1.5 Hydrogen	8
1.6 Natural Gas	9
1.7 Methane Activation	11
1.8 Methane Decomposition	13
1.9 Problem Statement	15
1.10 Objectives	17
1.11 Scope of the Study	18
1.12 Organization of the Thesis	20
<b>CHAPTER 2 - LITERATURE REVIEW</b>	22
2.1 Carbon Nanotubes	22
2.1.1 History of filamentous carbons	22
2.1.2 Structure of carbon nanotubes	24
2.1.3 Special properties of carbon nanotubes	25
2.1.3(a) Mechanical properties	25
2.1.3(b) Thermal conductivity and superconductivity properties	27
2.1.3(c) Electrical properties	28
2.1.4 The potential applications of carbon nanotubes	29
2.1.4(a) Catalyst support and adsorbent	29
2.1.4(b) Composites	31
2.1.4(c) Energy storage	31
2.1.4(d) Microelectronic and semiconductors	32
2.1.4(e) Biomedicine	32
2.2 Carbon Nanotubes Synthesis Methods	33
2.2.1 Electric-arc-discharge method	33
2.2.2 Laser ablation method	34
2.2.3 Catalytic growth method	36
2.2.4 Summary	37
2.3 Formation of Carbon Nanotubes via Catalysis Method	39
2.3.1 Catalytic growth of CNTs from various carbon sources	39
2.3.2 Catalytic growth of CNTs by methane decomposition	42
2.3.2(a) Advantages of using methane as a carbon source	42

2.3.2(b)	Effect of active metals and promoters in methane decomposition	43
2.3.2(c)	Effect of catalyst supports in methane decomposition	48
2.3.2(d)	Effect of reaction temperature in methane decomposition	50
2.4	Models of Metal-Support Interactions	52
2.5	Effect of Calcination Temperature	54
2.6	Effect of Hydrogen Pretreatment	54
2.7	Models of Catalytic Growth	56
2.7.1	Vapor-liquid-solid Theory	56
2.7.2	Carbon nanotubes growth mechanisms	57
2.7.2(a)	Tip growth and base growth model	58
2.7.2(b)	Base-tip growth model	59
2.8	Process and Kinetic Studies	60
2.8.1	Process study	60
2.8.2	Kinetic study	61
<b>CHAPTER 3 – MATERIALS AND METHODS</b>		<b>65</b>
3.1	Materials and Chemicals	65
3.2	Catalyst Activity Measurement	66
3.2.1	Experimental rig setup	66
3.2.1(a)	Gas mixing section	66
3.2.1(b)	Reaction section	70
3.2.1(c)	Gas analysis section	71
3.3	Overall Experimental Flowchart	72
3.4	Catalysts Preparation Methods	73
3.4.1	Impregnation method (IMP)	73
3.4.2	Co-precipitation method (Co-P)	73
3.4.3	Sol-gel method (SG)	74
3.5	Catalytic Activity Test and Preparation of Carbon Nanotubes	74
3.5.1	Preliminary studies on methane decomposition	75
3.5.2	Screening of suitable catalysts for methane decomposition	75
3.5.3	Methane decomposition over supported-NiO catalysts	77
3.5.4	Methane decomposition over supported-CoO <sub>x</sub> catalysts	78
3.5.5	Studies on the effect of catalyst preparation on methane decomposition over 8CoO <sub>x</sub> -2MoO <sub>x</sub> /Al <sub>2</sub> O <sub>3</sub> catalyst	79
3.6	Process Analysis and Optimization	81
3.7	Kinetic Study	83
3.8	Catalyst and Carbon Nanotubes Characterizations	83
3.8.1	Surface characteristics	83
3.8.2	Raman spectroscopy	83
3.8.3	Scanning electron microscopy (SEM)	84
3.8.4	Transmission electron microscopy (TEM)	84
3.8.5	Thermal gravimetric analysis (TGA)	85
3.8.6	Temperature-programmed reduction (TPR)	85
3.8.7	X-ray diffraction (XRD)	86
<b>CHAPTER 4 - RESULTS AND DISCUSSION</b>		<b>87</b>
4.1	Preliminary Study on Catalytic Decomposition of Methane	87
4.1.1	Blank test	87
4.1.2	Screening of transition metals	88

4.2	Methane Decomposition over Supported-Nickel Oxide Catalysts	90
4.2.1	Screening of catalyst supports	90
4.2.2	Examination of NiO supported on Al <sub>2</sub> O <sub>3</sub> , CeO <sub>2</sub> , H-ZSM-5 and SiO <sub>2</sub>	92
4.2.2(a)	Catalytic performances	92
4.2.2(b)	Characterizations of supported-NiO catalysts	94
4.2.2(c)	Characterizations of deposited carbons	97
4.2.2(d)	Formation of SWNTs on NiO/Al <sub>2</sub> O <sub>3</sub> catalyst	103
4.2.2(e)	Summary	106
4.2.3	Examination of NiO-M/SiO <sub>2</sub> catalysts	107
4.2.3(a)	Effect of catalyst promoters	107
4.2.3(b)	Effect of catalyst supports for NiO-CuO catalysts	109
4.2.3(c)	Effect of weight ratio of NiO to CuO	111
4.2.3(d)	Effect of NiO-CuO loadings	113
4.2.3(e)	Characterization of catalysts and deposited carbons	115
4.2.3(f)	Summary	121
4.2.4	Examination of NiO-CuO-M/SiO <sub>2</sub> catalysts	123
4.2.4(a)	TEM characterization	123
4.2.4(b)	Summary	126
4.3	Methane Decomposition over Supported-Cobalt Oxide Catalysts	127
4.3.1	Screening of catalyst supports	127
4.3.1(a)	TEM characterization	129
4.3.1(b)	Summary	131
4.3.2	Comparative study of NiO and CoO <sub>x</sub> supported on Al <sub>2</sub> O <sub>3</sub> and SiO <sub>2</sub>	132
4.3.2(a)	Carbon yield	132
4.3.2(b)	Carbon morphology	133
4.3.2(c)	XRD characterization	134
4.3.2(d)	TPR characterization	135
4.3.2(e)	Effect of MSI on carbon nanotubes formation	137
4.3.2(f)	Summary	138
4.3.3	Effect of promoters for CoO <sub>x</sub> /Al <sub>2</sub> O <sub>3</sub> catalyst	139
4.3.4	Effect of FeO <sub>x</sub> loadings on CoO <sub>x</sub> /Al <sub>2</sub> O <sub>3</sub> catalyst	142
4.3.5	Effect of MoO <sub>x</sub> loadings on CoO <sub>x</sub> /Al <sub>2</sub> O <sub>3</sub> catalyst	145
4.3.5(a)	Carbon yield	145
4.3.5(b)	TEM characterization	146
4.3.5(c)	XRD characterization	149
4.3.5(d)	Summary	152
4.4	Studies on the Effect of Catalyst Preparation on Methane Decomposition over 8CoO <sub>x</sub> -2MoO <sub>x</sub> /Al <sub>2</sub> O <sub>3</sub> catalyst	153
4.4.1	Effect of catalyst calcination temperature	153
4.4.1(a)	Carbon yield	153
4.4.1(b)	TEM characterization	154
4.4.1(c)	XRD characterization	159
4.4.1(d)	Summary	163
4.4.2	Effect of catalyst preparation methods	164
4.4.3	Effect of CoO <sub>x</sub> -MoO <sub>x</sub> loadings	166
4.4.3(a)	Carbon yield	166
4.4.3(b)	TEM characterization	167
4.4.3(c)	XRD characterization	171

4.4.4	Effect of catalyst reduction temperature	173
4.4.4(a)	Carbon yield	173
4.4.4(b)	TEM characterization	174
4.4.4(c)	Raman characterization	179
4.4.4(d)	XRD characterization	181
4.4.5(e)	Summary	183
4.5	Process Study and Analysis	184
4.5.1	Process analysis using COST	184
4.5.1(a)	Effect of reaction temperature	184
4.5.1(b)	Effect of partial pressure of methane	186
4.5.1(c)	Effect of catalyst weight	187
4.5.1(d)	Summary	188
4.5.2	Process analysis using factorial design of RSM	189
4.5.2(a)	Statistical analysis and modeling	191
4.5.2(b)	Effects of reaction temperature, partial pressure of methane and catalyst weight on carbon yield	193
4.5.3	Optimization study	196
4.5.3(a)	TGA characterization	197
4.5.3(b)	TEM and SEM characterizations	198
4.5.3(c)	Raman characterization	199
4.5.3(d)	Surface characterization	200
4.5.3(e)	Summary	204
4.5.4	Effects of reaction temperature and gas-hourly-space-velocity	205
4.5.4(a)	Carbon yield	205
4.5.4(b)	TEM characterization	206
4.5.4(c)	Raman characterization	209
4.5.4(d)	Summary	211
4.6	Kinetics Studies	212
4.6.1	Reaction order	212
4.6.2	Activation energy	214
4.6.3	Rate-determining step (RDS)	216
4.6.3(a)	Assumption that dissociative adsorption of methane be RDS	221
4.6.3(b)	Assumption that abstraction of second hydrogen atom be RDS	224
4.6.3(c)	Assumption that abstraction of third hydrogen atom be RDS	224
4.6.3(d)	Assumption that abstraction of fourth hydrogen atom be RDS	225
4.6.3(e)	Assumption that desorption of hydrogen atom be RDS	225
4.6.3(f)	Assumption that dissolution of carbon atom be RDS	226
4.6.3(g)	Summary	227
<b>CHAPTER 5 - CONCLUSIONS</b>		<b>228</b>
<b>CHAPTER 6 - RECOMMENDATIONS FOR FUTURE RESEARCH</b>		<b>232</b>
<b>BIBLIOGRAPHY</b>		<b>234</b>
<b>APPENDICES</b>		<b>252</b>
<b>LIST OF PUBLICATIONS</b>		<b>259</b>



## LIST OF TABLES

		Page
Table 1.1	Typical composition of natural gas (NaturalGas, 2007; GasMalaysia, 2008)	10
Table 2.1	A summary of the mechanical properties of CNTs in comparison with other materials (Lu and Han, 1998)	26
Table 2.2	Examples of CNTs used as catalyst supports in various reactions	30
Table 2.3	A short summary of the current three most common techniques used in producing CNTs (Daenen <i>et al.</i> , 2003)	38
Table 2.4	Summary of recent researches on the catalytic growth of CNTs from various carbon sources	40
Table 2.5	Summary of recent researches on the catalytic growth of CNTs by catalytic decomposition of methane	44
Table 2.6	Summary of the effects of process parameters on CNTs production	63
Table 2.7	Summary of kinetic study for methane decomposition over different catalytic materials	64
Table 3.1	List of chemicals and reagents	65
Table 3.2	Major components of the experimental rig and their functions	67
Table 3.3	Gas chromatography retention time data of each detected gas component	71
Table 3.4	Experimental conditions for methane decomposition based on 3-level factorial design using RSM	82
Table 4.1	Methane conversions recorded in a blank test study	87
Table 4.2	The performance of the silica-supported metal oxide catalysts for decomposition of methane at 550°C	89
Table 4.3	The performance of the silica-supported metal oxide catalysts for decomposition of methane at 700°C	89
Table 4.4	Carbon yields of supported-NiO catalysts after 180 min reaction at 550°C and after 60 min reaction at 700°C	94

Table 4.5	The average NiO crystallite size for supported-NiO catalysts	97
Table 4.6	Methane conversions up to 90 min reaction over 9NiO-1M catalysts supported on SiO <sub>2</sub> at 700°C	108
Table 4.7	Methane conversions up to 90 min reaction over 9NiO-1CuO on different supports at 700°C	110
Table 4.8	Catalytic properties of supported-CoO <sub>x</sub> catalysts in methane decomposition at 550°C	128
Table 4.9	Catalytic properties of supported-CoO <sub>x</sub> catalysts in methane decomposition at 700°C	129
Table 4.10	Carbon yields for CoO <sub>x</sub> /Al <sub>2</sub> O <sub>3</sub> , CoO <sub>x</sub> /SiO <sub>2</sub> , NiO/Al <sub>2</sub> O <sub>3</sub> and NiO/SiO <sub>2</sub> catalysts from methane decomposition at 550°C and 700°C	133
Table 4.11	Average diameters and standard deviations of CNTs synthesized at 550°C and 700°C	134
Table 4.12	Catalytic properties of promoted supported-CoO <sub>x</sub> catalysts in methane decomposition at 700°C	139
Table 4.13	Catalytic properties of tested catalysts in methane decomposition at 700°C	142
Table 4.14	The average sizes of cobalt oxide crystallites at different calcination temperatures	161
Table 4.15	Methane conversions over 8CoO <sub>x</sub> -2MoO <sub>x</sub> /Al <sub>2</sub> O <sub>3</sub> catalyst with different loadings of 8CoO <sub>x</sub> -2MoO <sub>x</sub> at 700°C	166
Table 4.16	The average sizes of cobalt oxide crystallites for different amounts of 8CoO <sub>x</sub> -2MoO <sub>x</sub> loading	172
Table 4.17	Experiment matrix of three-level factorial design of response surface methodology (RSM)	190
Table 4.18	Sequential model sum of squares	190
Table 4.19	ANOVA table of carbon yield	192
Table 4.20	The preset goal with the constraints for all the independent factors and responses in numerical optimization	196
Table 4.21	Reproducibility test under optimum condition over Co-Mo/Al <sub>2</sub> O <sub>3</sub> catalyst	197

Table 4.22	Physical properties of $\text{Al}_2\text{O}_3$ support, 8Co-2Mo/ $\text{Al}_2\text{O}_3$ catalyst and as-synthesized CNTs	201
Table 4.23	Values of reaction rate constant, k, at various reaction temperatures	215

## LIST OF FIGURES

		Page
Figure 1.1	Schematic diagram showing the typical catalyst structure used in a chemical reactor (Inano, 2007)	2
Figure 1.2	The diagram shows the nanotechnology region (Nanodimension, 2005)	3
Figure 1.3	The allotropes of carbon (Lau and Hui, 2002)	4
Figure 1.4	The structure of CNT with enclosed tip (Nanodimension, 2005)	6
Figure 1.5	Schematic diagrams for (a) SWNTs in bundle form and (b) MWNT with five graphene sheets	7
Figure 1.6	Schematic diagram presentation of the cross sections of (a,b) CNFs and (c) CNTs, with regard of their graphitic structures	8
Figure 1.7	Schematic diagram presentation of the cross sections of (a,b) CNFs and (c) CNTs, with regardless of their graphitic structures	8
Figure 1.8	Evolution of global market shares of different energy carriers for the period 2000 – 2100. The alcohol category includes methanol and ethanol (Barreto <i>et al.</i> , 2003)	9
Figure 1.9	Various paths of methane activation to more value-added products (Choudhary <i>et al.</i> , 2003)	12
Figure 1.10	Flowchart showing the possible products obtained from CDM process	14
Figure 2.1	The different structures of carbon allotropes: (a) fullerene (0-D), (b) carbon nanotubes (1-D), (c) graphite (2-D) and (d) diamond (3-D) (Cohen, 2001)	23
Figure 2.2	The two-dimensional graphene sheet given chiralities (n, m) (Dresselhaus and Avouris, 2001)	24
Figure 2.3	Schematic diagrams for CNTs with chiral vectors (a) $\theta = 30^\circ$ direction [an “armchair” (n, n) nanotube], (b) $\theta = 0^\circ$ direction [a “zigzag” (n, 0) nanotube] and (c) a general $\theta$ direction with $0 < \theta < 30^\circ$ [a “chiral” (n, m) nanotube] (Dresselhaus and Avouris, 2001)	25
Figure 2.4	Different adsorption sites in CNTs: (A) surface, (B) groove, (C) pores and (D) interstitial (Serp <i>et al.</i> , 2003)	31

Figure 2.5	Schematic reactor setup for electric-arc-discharge method	34
Figure 2.6	Schematic reactor setup for laser ablation method	35
Figure 2.7	Schematic reactor setup for catalytic growth method	37
Figure 2.8	The schematic diagram showing the CNTs grown on the surface of a catalyst	47
Figure 2.9	Graphical illustration of metal particle morphologies under influencing of (a) weak, (b) moderate and (c) strong MSI effect (Baker <i>et al.</i> , 1987)	53
Figure 2.10	Graphical illustration of vapor-liquid-solid theory	57
Figure 2.11	Graphical depiction of the possible CNTs growth models. (a) Tip growth model, (b) Base growth model and (c) Base-tip growth model	58
Figure 3.1	Schematic diagram of the experimental rig setup	68
Figure 3.2	Schematic diagram of fixed-bed reactor system	70
Figure 3.3	Flowchart of overall experimental activities involved in this study	72
Figure 3.4	Metals selected for catalyst development in this study	76
Figure 4.1	Hydrogen yields of supported-NiO catalysts for decomposition of methane at 550°C	90
Figure 4.2	Hydrogen yields of supported-NiO catalysts for decomposition of methane at 700°C	91
Figure 4.3	Changes of methane conversion as a function of time on stream over supported-NiO catalysts at (a) 550°C and (b) 700°C	93
Figure 4.4	TEM images of fresh catalysts. (a) NiO/SiO <sub>2</sub> , (b) NiO/HZSM-5, (c) NiO/CeO <sub>2</sub> and (d) NiO/Al <sub>2</sub> O <sub>3</sub>	95
Figure 4.5	XRD patterns of (a) NiO, (b) NiO/SiO <sub>2</sub> , (c) NiO/HZSM-5, (d) NiO/CeO <sub>2</sub> and (e) NiO/Al <sub>2</sub> O <sub>3</sub> . (▼) NiO, (◆) SiO <sub>2</sub> , (○) HZSM-5 (◇), CeO <sub>2</sub> , (●) Al <sub>2</sub> O <sub>3</sub>	96
Figure 4.6	TEM images of filamentous carbons produced on (a) NiO/SiO <sub>2</sub> , (b) NiO/HZSM-5, (c) NiO/CeO <sub>2</sub> and (d) NiO/Al <sub>2</sub> O <sub>3</sub> at 550°C	98

Figure 4.7	TEM images of filamentous carbons produced on (a) NiO/SiO <sub>2</sub> , (b) NiO/HZSM-5, (c) NiO/CeO <sub>2</sub> and (d) NiO/Al <sub>2</sub> O <sub>3</sub> at 700°C. Inset: SWNTs	99
Figure 4.8	Outer diameter distribution histograms of filamentous carbons synthesized over (a) NiO/SiO <sub>2</sub> , (b) NiO/HZSM-5, (c) NiO/CeO <sub>2</sub> and (d) NiO/Al <sub>2</sub> O <sub>3</sub> catalysts at 550°C	100
Figure 4.9	Outer diameter distribution histograms of filamentous carbons synthesized over (a) NiO/SiO <sub>2</sub> , (b) NiO/HZSM-5, (c) NiO/CeO <sub>2</sub> and (d) NiO/Al <sub>2</sub> O <sub>3</sub> catalysts at 700°C	101
Figure 4.10	TEM images of SWNTs in isolated form (arrow A1) and in bundles form (arrow A2) and a MWNT (arrow B)	104
Figure 4.11	Raman spectrum (excitation beam wavelength = 514.55 nm)	105
Figure 4.12	Hydrogen and carbon yields in methane decomposition over NiO/SiO <sub>2</sub> and 9NiO-1M/SiO <sub>2</sub> catalysts at 700°C	109
Figure 4.13	Hydrogen and carbon yields in methane decomposition over different supported 9NiO-1CuO catalysts at 700°C	111
Figure 4.14	Changes of methane conversions as a function of time on stream	112
Figure 4.15	Hydrogen and carbon yields in methane decomposition over NiO-CuO/SiO <sub>2</sub> catalysts with different weight ratios of NiO to CuO at 700°C	112
Figure 4.16	Methane conversion data as a function of time on stream with different loadings of 8NiO-2CuO on SiO <sub>2</sub> at 700°C	113
Figure 4.17	Hydrogen and carbon yields in methane decomposition over 8NiO-2CuO/SiO <sub>2</sub> catalyst with different loadings of 8NiO-2CuO at 700°C	115
Figure 4.18	XRD patterns of (A) fresh catalysts and (B) used catalyst: (a) NiO/SiO <sub>2</sub> , (b) 8NiO-2CuO/SiO <sub>2</sub> (10:90) and (c) 8NiO-2CuO/SiO <sub>2</sub> (80:20) (▼) NiO, (◆) CuO, (◇) SiO <sub>2</sub> , (●) graphite.	116
Figure 4.19	TGA profile of filamentous carbons over 8NiO-2CuO/SiO <sub>2</sub> (80:20) catalyst after methane decomposition	118
Figure 4.20	TEM images of filamentous carbons grown on (a) NiO/SiO <sub>2</sub> and (b) 8NiO-2CuO/SiO <sub>2</sub> (10:90) catalysts in methane decomposition at 700°C	119

Figure 4.21	SEM images of filamentous carbons grown on (a) NiO/SiO <sub>2</sub> and (b) 8NiO-2CuO/SiO <sub>2</sub> (10:90) catalysts in methane decomposition at 700°C	120
Figure 4.22	TEM images of filamentous carbons grown on 8NiO-2CuO/SiO <sub>2</sub> (80:20) catalyst in methane decomposition at 700°C	121
Figure 4.23	(a) Low-magnified and (b) high-magnified SEM images of filamentous carbons grown on 8NiO-2CuO/SiO <sub>2</sub> (80:20) catalyst in methane decomposition at 700°C	121
Figure 4.24	TEM images (a,b) Y-junction CNTs grown on 7NiO-2CuO-1MoO <sub>x</sub> /SiO <sub>2</sub> catalyst and (c,d) filamentous carbons grown on 7NiO-2CuO-1CoO <sub>x</sub> /SiO <sub>2</sub> and (d) 8NiO-2MoO <sub>x</sub> /SiO <sub>2</sub> catalysts, respectively at 700°C	124
Figure 4.25	Schematic diagrams showing the proposed sequential growth mechanism of straight (i, ii) and Y-junction (iii, iv) tubular carbon structures (Chai <i>et al.</i> , 2006b)	126
Figure 4.26	TEM images of CNTs grown from methane decomposition over (a,b) CoO <sub>x</sub> /SiO <sub>2</sub> , (c) CoO <sub>x</sub> /H-ZSM-5 and (d) CoO <sub>x</sub> /Al <sub>2</sub> O <sub>3</sub> catalysts at 550°C	130
Figure 4.27	TEM images of (a) CoO <sub>x</sub> /SiO <sub>2</sub> , (b) CoO <sub>x</sub> /H-ZSM-5, (c) CoO <sub>x</sub> /CeO <sub>2</sub> and (b) CoO <sub>x</sub> /Al <sub>2</sub> O <sub>3</sub> catalysts after methane decomposition at 700°C	131
Figure 4.28	XRD patterns of catalysts (a) NiO/SiO <sub>2</sub> , (b) NiO/Al <sub>2</sub> O <sub>3</sub> , (c) CoO <sub>x</sub> /SiO <sub>2</sub> and (d) CoO <sub>x</sub> /Al <sub>2</sub> O <sub>3</sub> . (▼) NiO, (◇) Co <sub>3</sub> O <sub>4</sub> , (●) SiO <sub>2</sub> and (○) Al <sub>2</sub> O <sub>3</sub>	134
Figure 4.29	TPR profiles of catalysts (a) NiO/SiO <sub>2</sub> , (b) NiO/Al <sub>2</sub> O <sub>3</sub> , (c) CoO <sub>x</sub> /SiO <sub>2</sub> and (d) CoO <sub>x</sub> /Al <sub>2</sub> O <sub>3</sub>	136
Figure 4.30	TEM images of CNTs grown from methane decomposition over the following bimetallic catalysts at 700°C. (a) 8CoO <sub>x</sub> -2NiO/Al <sub>2</sub> O <sub>3</sub> , (b) 8CoO <sub>x</sub> -2FeO <sub>x</sub> /Al <sub>2</sub> O <sub>3</sub> , (c) 8CoO <sub>x</sub> -2MoO <sub>x</sub> /Al <sub>2</sub> O <sub>3</sub> and (d) 8CoO <sub>x</sub> -2CuO/Al <sub>2</sub> O <sub>3</sub>	141
Figure 4.31	TEM images of CNTs grown on (a) CoO <sub>x</sub> /Al <sub>2</sub> O <sub>3</sub> , (b) 8CoO <sub>x</sub> -2FeO <sub>x</sub> /Al <sub>2</sub> O <sub>3</sub> , (c) 6CoO <sub>x</sub> -4FeO <sub>x</sub> /Al <sub>2</sub> O <sub>3</sub> and (d) 4CoO <sub>x</sub> -6FeO <sub>x</sub> /Al <sub>2</sub> O <sub>3</sub> at 700°C	143
Figure 4.32	Carbon yields in methane decomposition over CoO <sub>x</sub> -MoO <sub>x</sub> /Al <sub>2</sub> O <sub>3</sub> catalysts with different weight ratios of CoO <sub>x</sub> to MoO <sub>x</sub> at 700°C	146

Figure 4.33	(Left) Histogram of diameter distributions and (right) TEM images of CNTs produced on $\text{CoO}_x\text{-MoO}_x/\text{Al}_2\text{O}_3$ catalysts with weight ratios of $\text{CoO}_x$ to $\text{MoO}_x$ at (a) 9:1, (b) 8:2, (c) 7:3, (d) 6:4 and (e) 4:6, respectively	147
Figure 4.34	Plot of the average diameters $\pm$ standard deviations of CNTs produced on $\text{CoO}_x\text{-MoO}_x/\text{Al}_2\text{O}_3$ catalysts with different weight ratios of $\text{CoO}_x$ to $\text{MoO}_x$	149
Figure 4.35	XRD patterns of $\text{CoO}_x\text{-MoO}_x/\text{Al}_2\text{O}_3$ catalysts with weight ratio of $\text{CoO}_x$ to $\text{MoO}_x$ at (a) 8:2, (b) 6:4, (c) 4:6 and (d) 2:8 (w/w), respectively. ( $\diamond$ ) $\text{Co}_3\text{O}_4$ , ( $\circ$ ) $\text{Al}_2\text{O}_3$ , ( $\nabla$ ) $\text{CoMoO}_4$ , ( $\Delta$ ) $\text{MoO}_3$ .	150
Figure 4.36	Scheme illustrating the surface structural model proposed for (a) $\text{CoO}_x/\text{Al}_2\text{O}_3$ and (b-d) $\text{CoO}_x\text{-MoO}_x/\text{Al}_2\text{O}_3$ with increased weight ratios of $\text{CoO}_x$ to $\text{MoO}_x$	152
Figure 4.37	Carbon yield as a function of catalyst calcination temperature	154
Figure 4.38	Plot of the average diameters $\pm$ standard deviations of CNTs as a function of catalyst calcination temperature	155
Figure 4.39	(Left) Histogram of CNTs diameter distributions and (right) TEM images of CNTs grown on $8\text{CoO}_x\text{-2MoO}_x/\text{Al}_2\text{O}_3$ catalyst, calcined at (a) $300^\circ\text{C}$ , (b) $450^\circ\text{C}$ , (c) $600^\circ\text{C}$ , (d) $650^\circ\text{C}$ and (e) $700^\circ\text{C}$ , respectively	156
Figure 4.40	HRTEM image of CNTs grown on $8\text{CoO}_x\text{-2MoO}_x/\text{Al}_2\text{O}_3$ catalyst, calcined at $700^\circ\text{C}$	159
Figure 4.41	XRD patterns of $8\text{CoO}_x\text{-2MoO}_x/\text{Al}_2\text{O}_3$ catalyst calcined at (a) $300^\circ\text{C}$ , (b) $450^\circ\text{C}$ , (c) $600^\circ\text{C}$ , (d) $700^\circ\text{C}$ and (e) $750^\circ\text{C}$ ( $\diamond$ ) $\text{Co}_3\text{O}_4$ or $\text{CoAl}_2\text{O}_4$ , ( $\circ$ ) $\text{Al}_2\text{O}_3$ , ( $\nabla$ ) $\text{CoMoO}_4$ .	160
Figure 4.42	Scheme illustrating the surface structural model proposed for the strong interaction between $\text{Al}_2\text{O}_3$ and $\text{CoO}_x$ leading to the formation of $\text{Co}_3\text{O}_4$ at calcination temperatures $\text{CoAl}_2\text{O}_4$ at $\leq 700^\circ\text{C}$ and $\text{CoAl}_2\text{O}_4$ at $\geq 750^\circ\text{C}$	163
Figure 4.43	Carbon yields in methane decomposition over $8\text{CoO}_x\text{-2MoO}_x/\text{Al}_2\text{O}_3$ catalyst with different loadings of $8\text{CoO}_x\text{-2MoO}_x$ up to 180 min reaction at $700^\circ\text{C}$ .	167
Figure 4.44	(Left) Histograms of diameter distributions of CNTs and (right) TEM images of CNTs grown on $8\text{CoO}_x\text{-2MoO}_x/\text{Al}_2\text{O}_3$ catalyst with $8\text{CoO}_x\text{-2MoO}_x$ loading of (a) 5 wt%, (b) 20 wt%, (c) 30 wt%, (d) 50 wt% and (e) 70 wt%, respectively	168



Figure 4.45	Plot of the average diameters $\pm$ standard deviations of CNTs as a function of $8\text{CoO}_x\text{-}2\text{MoO}_x$ loadings	171
Figure 4.46	XRD patterns of $8\text{CoO}_x\text{-}2\text{MoO}_x/\text{Al}_2\text{O}_3$ catalyst with $8\text{CoO}_x\text{-}2\text{MoO}_x$ loading of (a) 5 wt%, (b) 10 wt%, (c) 30 wt%, (d) 50 wt% and (f) 70 wt%, respectively. ( $\diamond$ ) $\text{Co}_3\text{O}_4$ , ( $\circ$ ) $\text{Al}_2\text{O}_3$ , ( $\nabla$ ) $\text{CoMoO}_4$	172
Figure 4.47	Carbon yields over (a) unreduced catalyst and catalysts reduced at (b) $400^\circ\text{C}$ , (c) $550^\circ\text{C}$ and (d) $700^\circ\text{C}$ , respectively.	174
Figure 4.48	Low-magnified TEM images of CNTs grown on (a) unreduced catalyst and catalysts reduced at (b) $400^\circ\text{C}$ , (c) $550^\circ\text{C}$ and (d) $700^\circ\text{C}$ , respectively	175
Figure 4.49	High-magnified TEM images of CNTs grown on (a) unreduced catalyst and (b) catalyst reduced at $550^\circ\text{C}$	175
Figure 4.50	Histograms of diameter distributions for CNTs grown on (a) unreduced catalyst and catalysts reduced at (b) $400^\circ\text{C}$ , (c) $550^\circ\text{C}$ , and (d) $700^\circ\text{C}$ , respectively	176
Figure 4.51	Plot of the average diameters $\pm$ standard deviations of CNTs	177
Figure 4.52	TEM images of $8\text{Co-}2\text{Mo}/\text{Al}_2\text{O}_3$ catalysts: (a) unreduced catalyst and catalysts reduced at (b) $400^\circ\text{C}$ , (c) $550^\circ\text{C}$ and (d) $700^\circ\text{C}$ , respectively. All figures are on the same scale	178
Figure 4.53	Raman spectra for CNTs grown on (a) unreduced catalyst and catalysts reduced at (b) $400^\circ\text{C}$ , (c) $550^\circ\text{C}$ and (d) $700^\circ\text{C}$ , respectively	179
Figure 4.54	Changes in the $I_D/I_G$ ratio for CNTs as a function of reduction temperature	180
Figure 4.55	XRD patterns of $\text{Co-Mo}/\text{Al}_2\text{O}_3$ catalysts: (a) unreduced catalyst, (b) unreduced catalyst after methane decomposition at $700^\circ\text{C}$ , (c) catalyst after $\text{H}_2$ reduction at $550^\circ\text{C}$ for 1 h and (d) reduced catalyst after methane decomposition at $700^\circ\text{C}$	182
Figure 4.56	(a) Kinetic curves of methane conversion as a function of time and (b) carbon yield as a function of reaction temperatures $P_{\text{CH}_4} = 0.5 \text{ atm}$ and $W = 0.2 \text{ g}$	185
Figure 4.57	(a) Kinetic curves of methane conversion as a function of time and (b) carbon yield as a function of partial pressure of methane. $T = 750^\circ\text{C}$ and $W = 0.2 \text{ g}$	186

Figure 4.58	(a) Kinetic curves of methane conversion as a function of time and (b) carbon yield as a function of catalyst weight $T = 750^{\circ}\text{C}$ and $P_{\text{CH}_4} = 0.5 \text{ atm}$	188
Figure 4.59	Parity plot of actual and predicted values of carbon yield	193
Figure 4.60	Response surface plots for the effects of reaction temperature and $P_{\text{CH}_4}$ on carbon yield. (a) $W = 0.2 \text{ g}$ and (b) $W = 0.4 \text{ g}$	194
Figure 4.61	Response surface plots for the effects of partial pressure and catalyst weight on carbon yield. (a) $T = 700^{\circ}\text{C}$ and (b) $T = 800^{\circ}\text{C}$	194
Figure 4.62	Response surface plots for the effects of reaction temperature and catalyst weight on carbon yield. (a) $P_{\text{CH}_4} = 0.25 \text{ atm}$ and (b) $P_{\text{CH}_4} = 0.75 \text{ atm}$	194
Figure 4.63	TGA profile of CNTs synthesized over $8\text{Co-2Mo}/\text{Al}_2\text{O}_3$ catalyst after methane decomposition at optimum condition	198
Figure 4.64	(a) TEM image and (b) SEM image of CNTs grown on $8\text{Co-2Mo}/\text{Al}_2\text{O}_3$ catalyst at optimum condition. Inset: Open tips of CNTs	199
Figure 4.65	Raman spectrum of CNTs grown on $8\text{Co-2Mo}/\text{Al}_2\text{O}_3$ catalyst at optimum condition	200
Figure 4.66	Pore size distribution curves of (a) $\text{Al}_2\text{O}_3$ , (b) $8\text{Co-2Mo}/\text{Al}_2\text{O}_3$ and (c) as-synthesized CNTs	202
Figure 4.67	TEM image showing the open tips of CNTs grown on $8\text{Co-2Mo}/\text{Al}_2\text{O}_3$ catalyst	203
Figure 4.68	Schematic structural model for the aggregated pores	204
Figure 4.69	The effects of reaction temperature and GHSV on carbon yield after 2 h reaction over $8\text{Co-2Mo}/\text{Al}_2\text{O}_3$ catalyst	206
Figure 4.70	The effects of reaction temperature and GHSV on the average diameters of CNTs synthesized at $700^{\circ}\text{C}$ and $800^{\circ}\text{C}$ , respectively. Inset: Standard deviations of diameter distribution of CNTs	208
Figure 4.71	TEM images of CNTs synthesized at (a) $700^{\circ}\text{C}$ and (b) $800^{\circ}\text{C}$ , respectively. $\text{GHSV} = 9000 \text{ ml/h.g}_{\text{cat}}$	208

Figure 4.72	Raman spectra of CNTs synthesized at temperature ( $^{\circ}\text{C}$ ) and GHSV ( $\text{ml/h.g}_{\text{cat}}$ ) of (a) 700 and 18000, (b) 700 and 9000, (c) 700 and 6000, (d) 700 and 3000, (e) 800 and 18000, (f) 800 and 9000, (g) 800 and 6000, (h) 800 and 3000, respectively	209
Figure 4.73	Changes in the $I_{\text{D}}/I_{\text{G}}$ ratio for CNTs as a function of GHSV at both $700^{\circ}\text{C}$ and $800^{\circ}\text{C}$	210
Figure 4.74	Logarithm plot of methane partial pressure and initial reaction rate for methane decomposition over $8\text{Co-2Mo}/\text{Al}_2\text{O}_3$ catalyst at $700^{\circ}\text{C}$ , $750^{\circ}\text{C}$ , $775^{\circ}\text{C}$ and $800^{\circ}\text{C}$	213
Figure 4.75	Arrhenius plot of $\ln k$ as a function of $1/T$ over $8\text{Co-2Mo}/\text{Al}_2\text{O}_3$ catalyst	215
Figure 4.76	Graphical illustration demonstrating the proposed mechanism of CNTs formation over $8\text{Co-2Mo}/\text{Al}_2\text{O}_3$ catalyst via methane decomposition	217
Figure 4.77	Plots of initial reaction rates, $r_0$ , as a function of $P_{\text{CH}_4}$ over $8\text{Co-2Mo}/\text{Al}_2\text{O}_3$ catalyst at $700^{\circ}\text{C}$ , $750^{\circ}\text{C}$ and $800^{\circ}\text{C}$ $W = 0.4 \text{ g}$	223
Figure 4.78	Plot of the initial reaction rate as a function of $P_{\text{CH}_4}$ for dissolution of carbon atom into the cobalt particle be RDS	227
Figure 4.79	A conceptual model depicting dissociative adsorption of methane on the catalyst active sites	227
Figure A.1	Gas chromatography data of purified air	253
Figure A.2	XRD spectrum of $8\text{NiO-2CuO}/\text{SiO}_2$ catalyst	254
Figure A.3	TGA profile of CNFs synthesized over $8\text{NiO-2CuO}/\text{SiO}_2$ (80:20) catalyst at $700^{\circ}\text{C}$	255
Figure A.4	Raman spectrum of SWNTs synthesized over $\text{NiO}/\text{Al}_2\text{O}_3$ catalyst at $700^{\circ}\text{C}$	256
Figure A.5	TPR profile of $\text{NiO}/\text{Al}_2\text{O}_3$ catalyst	257
Figure A.6	Pore size distribution curve of CNTs synthesized over $8\text{CoO}_x\text{-2MoO}_x/\text{Al}_2\text{O}_3$ catalyst at optimum process condition	258

## LIST OF PLATES

		Page
Plate 3.1	Experimental rig setup and the major components of the rig	69
Plate 4.1	$8\text{CoO}_x\text{-}2\text{MoO}_x/\text{Al}_2\text{O}_3$ catalyst prepared with different methods and at different calcination temperatures: (a) Co-P, $700^\circ\text{C}$ , (b) SG, $700^\circ\text{C}$ , (c) IMP, $700^\circ\text{C}$ and (d) IMP, $750^\circ\text{C}$	165

## LIST OF ABBREVIATIONS

BEI	Back-scattering electron imaging
BET	Brunauer-Emmett-Teller
BJH	Barrett, Joyner and Halenda
BOC	British Oxygen Company
CDM	Catalytic decomposition of methane
CNFs	Carbon nanofibers
CNTs	Carbon nanotubes
Conv.	Conversion
Co-P	Co-precipitation
CO <sub>2</sub> RM	Carbon dioxide reforming of methane
COST	Change one separate factor at a time
CVD	Chemical vapor deposition
D	Dimension
DWNTs	Double-walled carbon nanotubes
EAD	Electric-arc-discharge
GC	Gas chromatography
FCs	Filamentous carbons
FID	Flame ionization detector
FT	Fischer-Tropsch (FT)
FWHM	Full width half maximum
HRTEM	High-resolution transmission electron microscopy
GHSV	Gas-hourly-space velocity
GTL	Gas to liquid
IMP	Impregnation
LA	Laser ablation
MOX	Malaysian Oxygen Berhad
MSI	Metal-support interaction
MTG	Methanol to gasoline
MWNTs	Multi-walled carbon nanotubes
OCM	Oxidative coupling of methane
POM	Partial oxidation of methane

RBM	Radial breathing mode
RDS	Rate-determining step
RSM	Response surface methodology
SEI	Secondary electron imaging
SEM	Scanning electron microscopy
SG	Sol-gel
SMSI	Strong metal-support interaction
SRM	Steam reforming of methane
SWNTs	Single-walled carbon nanotubes
Syngas	Synthesis gas
TCD	Thermal conductivity detector
TDM	Thermal decomposition of methane
TEM	Transmission electron microscopy
Temp.	Temperature
TGA	Thermogravimetric analysis
TPR	Temperature programmed reduction
VLS	Vapor-liquid-solid
WMSI	Weak metal-support interaction
XRD	X-ray diffraction
ZSM-5	Zeolite Socony Mobil-five

## LIST OF SYMBOLS

$C_S$	Surface carbon
$C_{Co,f}$	Concentration of carbon dissolved in at the front side of cobalt particle
$C_{Co,r}$	Concentration of carbon dissolved in at the rear side of cobalt particle
$C_T$	Total concentration of active sites
$C_V$	Concentration of vacant sites
$D$	Diameter (nm)
$E_a$	Activation energy (kJ/mol)
$k$	Rate constant ( $g_C/g_{metal}\cdot min\cdot atm$ )
$k_{+1}, k_{-1}, k_{+2}, k_{-2}, k_{+3}, k_{-3}, k_{+4}, k_{-4}, k_{+5}, k_{-5}, k_{+6}, k_{-6}$	Rate coefficients of the forward and reverse reactions
$K_1, K_2, K_3, K_4, K_5, K_6$	Equilibrium coefficients
$P_{CH_4}$	Partial pressure of methane (atm)
$P_{H_2}$	Partial pressure of hydrogen (atm)
$R$	Ideal gas law constant (8.314 J/mol.K)
$r_0$	Initial reaction rate ( $g_C/g_{metal}\cdot min$ )
$S$	Surface active site
$T$	Reaction temperature ( $^{\circ}C$ )
$X_{CH_4}$	Conversion of methane (%)
$W$	Catalyst weight (g)

### Greek symbols

$\theta$	Diffraction angle (rad)
$\omega$	Raman shift ( $cm^{-1}$ )
$\beta$	Full width half maximum (FWHM) (rad)
$\lambda$	X-ray wavelength ( $\text{\AA}$ )
$\tau$	Thickness of nanotube wall (nm)
$\alpha$	Frequency factor in Arrhenius equation
$\alpha-Al_2O_3$	Alpha alumina
$\gamma-Al_2O_3$	Gamma alumina

**PERANAN MANGKIN LOGAM TERSOKONG DAN PENCIRIAN  
MANGKIN DALAM PENGURAIAN METANA BERMANGKIN BAGI  
PEMBENTUKAN NANOTIUB KARBON SERAGAM  
DALAM PROSES SATU LANGKAH**

**ABSTRAK**

Nanotub karbon (CNTs) menarik perhatian para saintis di seluruh dunia kerana dimensi, kekuatan dan sifat-sifat fizikal yang istimewa membuatnya satu bahan yang unik dengan banyak aplikasi. Pelbagai kaedah sintesis CNTs telah dibangunkan dan di antaranya kaedah tumbesaran bermangkin muncul sebagai satu kaedah terjamin dalam penghasilan CNTs yang tinggi. Walaubagaimanapun, kaedah tumbesaran bermangkin masih menghadapi banyak cabaran dan usaha-usaha mengatasi cabaran tersebut merupakan tumpuan utama projek ini. Dalam penyelidikan ini, penguraian metana bermangkin telah digunakan untuk menghasilkan CNTs. Mangkin-mangkin monologam dan dwilogam turut disediakan daripada logam peralihan seperti Cr, Mn, Fe, Co, Ni, Cu, Mo dan Ag, dan disokong pada  $Al_2O_3$ ,  $CeO_2$ ,  $CaO$ , H-ZSM-5,  $La_2O_3$ ,  $MgO$ ,  $TiO_2$  dan  $SiO_2$ . Sifat-sifat mangkin yang dibangunkan ini diuji di dalam reaktor lapisan tetap tahan karat pada tekanan atmosfera. Pelbagai ujikaji pencirian termasuklah kaedah penurunan berprogramkan suhu (TPR), mikroskop elektron imbasan (SEM), mikroskop elektron transmisi (TEM), analisis pemetaan graviti haba (TGA), analisis permukaan dan kespektroskopan Raman telah dijalankan pada mangkin baru dan mangkin terpakai untuk mengetahui ciri-ciri CNTs yang dihasilkan dan kriteria yang diperlukan untuk membentuk CNTs yang berkualiti tinggi. Beberapa penemuan penting telah dikenalpasti di dalam penyelidikan ini. Di antaranya morfologi filamen karbon boleh disediakan secara khusus dengan menetapkan komponen mangkin dan menjalankan



tindakbalas dalam keadaan yang bersesuaian. Penemuan ini juga menunjukkan bahawa mangkin  $8\text{NiO}-2\text{CuO}/\text{SiO}_2$  dengan kandungan 80 wt% NiO-CuO menghasilkan nanofiber karbon (CNFs) dan hidrogen dalam kuantiti yang tinggi, iaitu dengan hasil karbon sebanyak  $143 \text{ g}_C/\text{g}_{(\text{NiO}+\text{CuO})}$  dan hasil hidrogen  $2344 \text{ mol H}_2/\text{mol (NiO+CuO)}$ . Nanotub karbon berdinding tunggal (SWNTs) dengan kememilihan yang tinggi juga dihasilkan oleh mangkin  $\text{NiO}/\text{Al}_2\text{O}_3$  pada suhu tindakbalas serendah  $700^\circ\text{C}$  dan CNTs berstruktur Y ditemui pada mangkin  $7\text{NiO}-2\text{CuO}-1\text{MoO}_x/\text{SiO}_2$ . Penyelidikan ini juga menunjukkan bahawa suhu pengkalsinan bagi mangkin adalah faktor penting dalam penentuan hasil dan morfologi CNTs terbentuk. Mangkin  $8\text{CoO}_x-2\text{MoO}_x/\text{Al}_2\text{O}_3$  yang dikalsinkan pada  $700^\circ\text{C}$  telah dikenalpasti berupaya menghasilkan nanotub karbon berdinding lapisan (MWNTs) dengan kawalan baik dari segi taburan diameternya, iaitu  $9.0 \pm 1.4 \text{ nm}$ . Kajian rawatan awal mangkin juga menunjukkan bahawa mangkin selepas diturunkan oleh hidrogen adalah lebih aktif dan suhu penurunan yang optimum adalah pada  $550^\circ\text{C}$ . Suhu tindakbalas dan tekanan separa metana juga dikenalpasti mempengaruhi hasil karbon bagi mangkin  $8\text{Co}-2\text{Mo}/\text{Al}_2\text{O}_3$  dengan ketara, sebaliknya faktor kuantiti mangkin yang digunakan adalah tidak ketara. Program rekabentuk eksperimen (DoE) menunjukkan proses yang optimum bagi penguraian metana bermangkin adalah pada suhu  $761^\circ\text{C}$ , tekanan separa metana  $0.75 \text{ atm}$  dan kuantiti mangkin  $0.4 \text{ g}$  dengan hasil karbon sebanyak 607%. Kajian kinetik juga menunjukkan bahawa penguraian metana bermangkin oleh mangkin  $8\text{Co}-2\text{Mo}/\text{Al}_2\text{O}_3$  adalah tertib pertama dengan tenaga pengaktifan  $87 \text{ kJ/mol}$ . Analisis seterusnya mendedahkan bahawa penjerapan terurai merupakan langkah penentuan kadar bagi penguraian metana oleh mangkin  $8\text{Co}-2\text{Mo}/\text{Al}_2\text{O}_3$ .

**ROLE OF METAL SUPPORTED CATALYSTS AND THEIR  
CHARACTERIZATION IN THE CATALYTIC DECOMPOSITION OF  
METHANE FOR THE FORMATION OF UNIFORM CARBON  
NANOTUBES IN A SINGLE STEP PROCESS**

**ABSTRACT**

Carbon nanotubes (CNTs) have attracted the fancy of many scientists worldwide due to their small dimensions, strength and remarkable properties that make them a very unique material of a whole range of promising applications. Many methods have been proposed to synthesize CNTs of which the catalytic growth method appears to be the most promising method for high yield synthesis of CNTs. However, there still lie many challenges in the catalytic growth method which is the main concern of this project. In this study, catalytic decomposition of methane was employed for producing CNTs. A number of monometallic and bimetallic catalysts were developed from transition metals, such as Cr, Mn, Fe, Co, Ni, Cu, Mo and Ag, on different supports of Al<sub>2</sub>O<sub>3</sub>, CeO<sub>2</sub>, CaO, H-ZSM-5, La<sub>2</sub>O<sub>3</sub>, MgO, TiO<sub>2</sub> and SiO<sub>2</sub>. The varied catalytic properties of these materials were examined in a vertical fixed-bed tubular reactor for methane decomposition. Various characterization tests, including surface characteristics, temperature-programmed reduction (TPR), X-ray diffraction (XRD), scanning electron microscopy (SEM), transmission electron microscopy (TEM), thermogravimetry analysis (TGA) and Raman spectroscopy, were carried out on the fresh and used catalysts in order to comprehend the properties of the produced CNTs and the criteria required to grow higher quality CNTs in high yield. Many illustrious findings were obtained in this study, one of which showed that various types of filamentous carbons could be tailor-made through proper designing of the catalyst components at the suitable reaction

conditions. It was also found in this study that 8NiO-2CuO/SiO<sub>2</sub> catalyst with 80 wt% of NiO-CuO loading produced carbon nanofibers (CNFs) and hydrogen of the highest yields, representing the yields of 143 g<sub>C</sub>/g<sub>(NiO+CuO)</sub> and 2344 mol H<sub>2</sub>/mol (NiO+CuO), respectively. Single-walled CNTs (SWNTs) were produced in high selectivity over NiO/Al<sub>2</sub>O<sub>3</sub> catalyst at a temperature as low as 700°C and Y-junction CNTs were found grown on 7NiO-2CuO-1MoO<sub>x</sub>/SiO<sub>2</sub> catalyst. The study also demonstrated that the effect of catalyst calcination temperature on the yield and the morphology of the produced CNTs was momentous. In this regard, 8CoO<sub>x</sub>-2MoO<sub>x</sub>/Al<sub>2</sub>O<sub>3</sub> catalyst, calcined at 700°C, grew multi-walled CNTs (MWNTs) with the best control of diameter distribution, i.e. 9.0 ± 1.4 nm. The catalyst pretreatment study disclosed that the catalyst was more active for the growth of CNTs after being reduced by hydrogen and the optimum reduction temperature was found to be 550°C. An examination of the process parameters for methane decomposition over reduced 8Co-2Mo/Al<sub>2</sub>O<sub>3</sub> catalyst showed that reaction temperature and methane partial pressure affected significantly the yield of carbon formation, whereas the effect of catalyst weight was insignificant. As predicted by Design of Experiment (DoE), the optimum process conditions for methane decomposition were found to be a temperature of 761°C, methane partial pressure of 0.75 atm and catalyst weight of 0.4 g, which give the highest carbon yield of 607%. Kinetic studies showed that methane decomposition reaction is first order with activation energy of 87 kJ/mol over 8Co-2Mo/Al<sub>2</sub>O<sub>3</sub> catalyst. An analysis of possible mechanisms showed that dissociative adsorption of methane is the rate-determining step for methane decomposition over 8Co-2Mo/Al<sub>2</sub>O<sub>3</sub> catalyst.

# CHAPTER 1

## INTRODUCTION

### 1.1 Catalysis

Catalysis involves the modification of the rate of a chemical reaction, usually a speeding up of the reaction rate, by addition of a substance, known as “catalyst”. According to the definition of Berzelius, a catalyst is a substance that accelerates the establishment of a chemical equilibrium without itself being consumed (Berzelius, 1836; Fogler, 1999). In general, catalysts can be categorized into three major groups, representing homogeneous catalysts, heterogeneous catalysts and biocatalysts (enzyme).

Heterogeneous catalysts, in particular supported catalysts, are important both from an industrial and a scientific point of view. These catalysts are widely used in many chemical processes such as catalytic reforming, hydrotreatment, polymerization reaction, hydrocracking, decomposition reaction and hydrogenation. Although most production processes using supported catalysts are carried out in a large-scale reactor, the reactions that actually take place in the catalysts occur on the surface of highly dispersed metal particles. The typical dimensions of these particles range from 1 nm to 100 nm (Figure 1.1), which by today’s standard are nanomaterials. Knowing that most of the catalysts have nanosized metal components, catalysis research and catalyst-based technologies have perhaps been at the heart of nanotechnology for many years. Nowadays, nanostructured catalysts receive a great demand in the petroleum and chemical processing industries. It is estimated that nanostructured catalysts will have an annual impact of USD 100 billion by 2015 (Roco and Bainbridge, 2001).

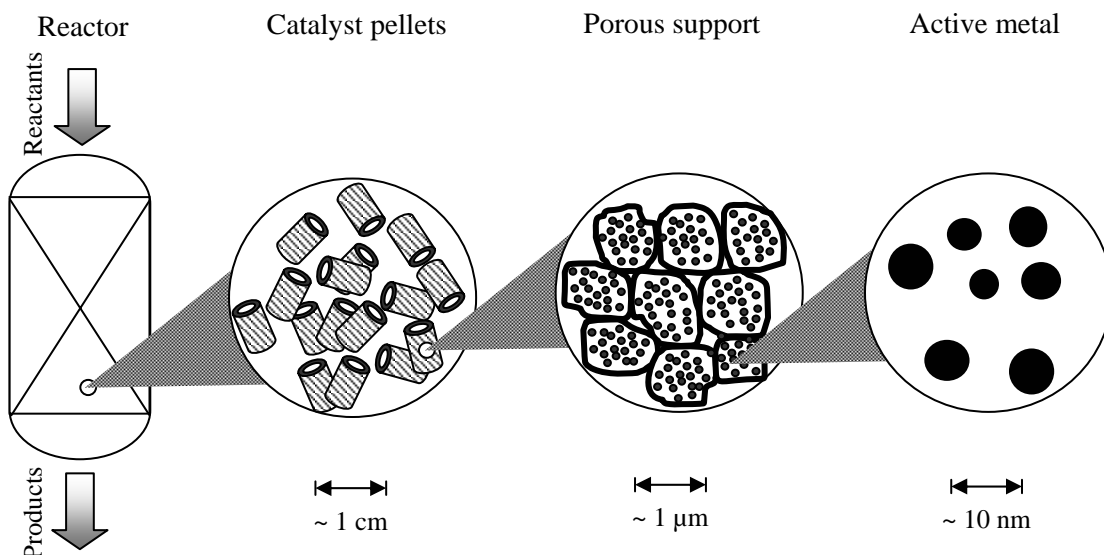


**Figure 1.1.** Schematic diagram showing the typical catalyst structure used in a chemical reactor (Inano, 2007).

## 1.2 Nanotechnology

Nanotechnology has emerged as one of the most exciting fields recently resulted from an integration of basic sciences like chemistry, physics, biology and mathematics with engineering sciences. The prefix “*nano*” in the world nanotechnology means a billionth ( $1 \times 10^{-9}$ ). According to Roco (2001), nanotechnology covenants with materials and systems having the following key properties:

- they have at least one dimension of about 1 – 100 nm
- they are designed through processes that exhibit fundamental control over the physical and chemical attributes of molecular-scale structure
- they can be combined to form larger structures

Nanotechnology is an important tool to control the processes in which materials are made and the manner devices function at the atomic and molecular

level. This level of control enables unlimited creation of new materials and new devices. In addition, the properties of traditional materials change at the nanoscale level, where the behavior of the surface starts to dominate over the behavior of the bulk phase. Thus, nanomaterials possess excellent and unique properties which cannot be found in any traditional materials in the bulk phase. Figure 1.2 presents a diagram showing the region that belongs to nanotechnology.

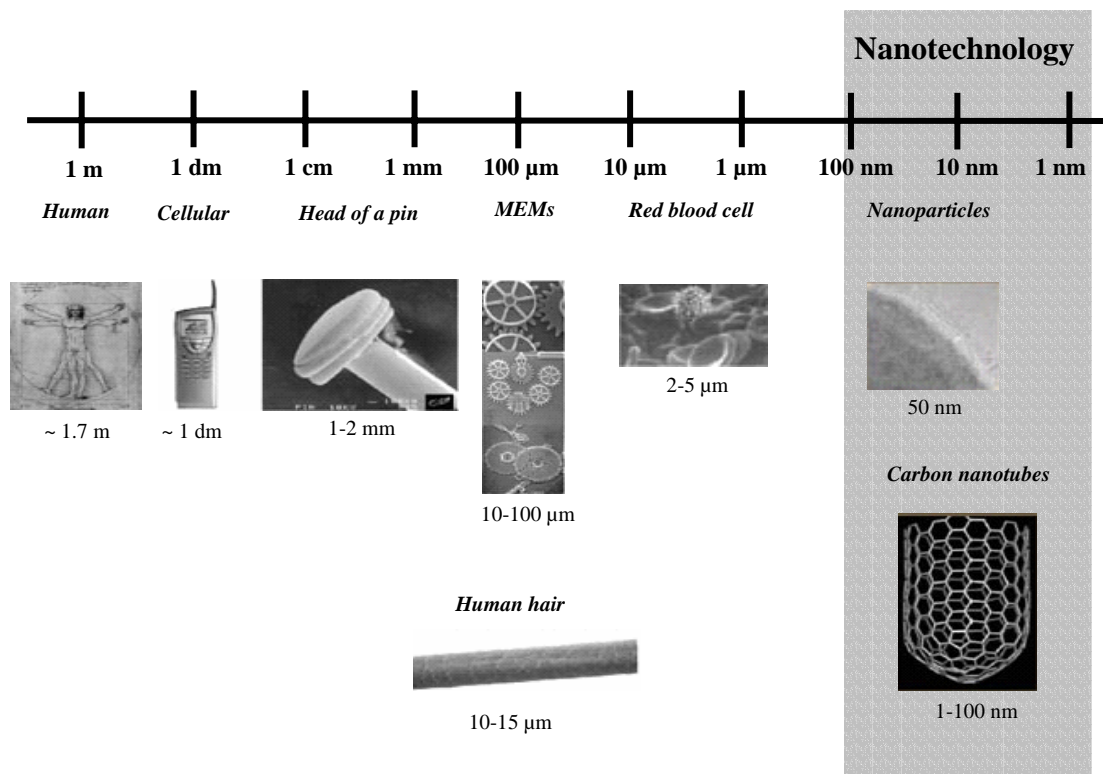


**Figure 1.2.** The diagram shows the nanotechnology region (Nanodimension, 2005).

The 21<sup>st</sup> century will undoubtedly be a period of substantial progress for nanotechnology. It is strongly believed that nanotechnology will complement and change life science, pharma, diagnostic, medicine technology, food, environmental technology, water, energy, electronics, mechanical engineering and so on to a new dimension in a near future. As reported by Roco and Bainbridge (2001), the market value of nano products and services will reach USD 1 trillion by 2015.

### 1.3 Allotropes of Carbon

Advances in nanotechnology have led to the discovery of a growing number of new materials. Carbon nanotubes (CNTs), the newly-discovered carbon allotrope, have emerged as one of the most important components of the nanotechnology.

It is widely known that carbon is an important element of unique properties with each carbon atom has six electrons, which occupy  $1s^2$ ,  $2s^2$  and  $2p^2$  atomic orbitals. These atomic orbitals give three possible hybridizations in carbon bonding, representing  $sp$ ,  $sp^2$  and  $sp^3$  configurations. Bonding of carbon atoms with neighbor atoms via  $sp$  configuration gives rise to chain structures,  $sp^2$  bonding to planar structures and  $sp^3$  bonding to tetrahedral structures. These hybridizations in carbon bonding are responsible for the formation of different carbon allotropes, including diamond (3-D form), graphite (2-D form), fullerene (0-D form) and recently CNTs (1-D form). The structures of these carbon allotropes are shown in Figure 1.3.

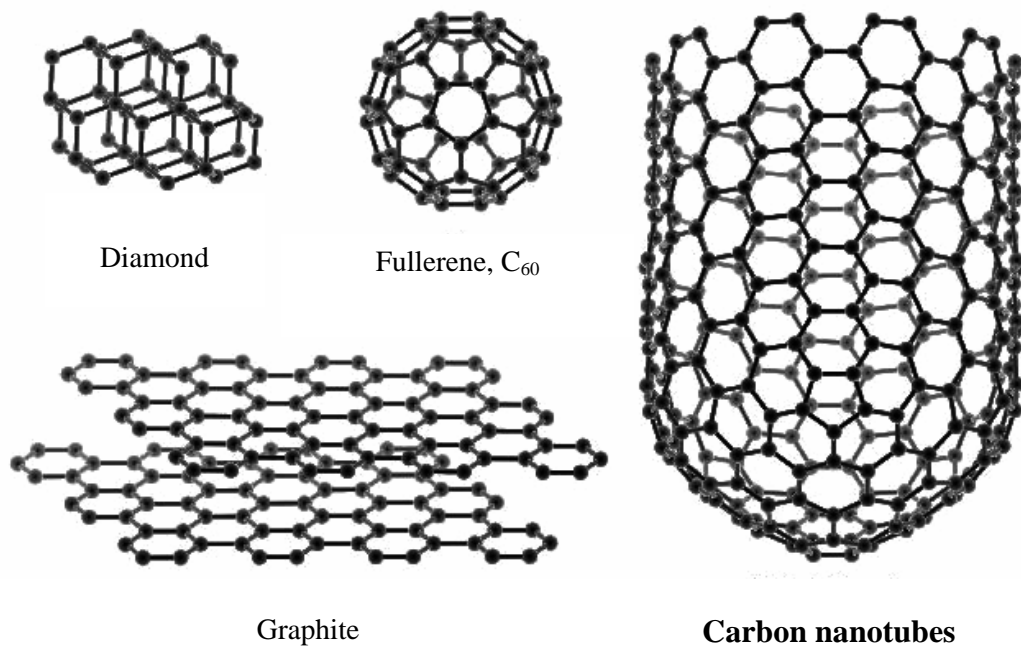


**Figure 1.3.** The allotropes of carbon (Lau and Hui, 2002).

Before 1985, it is commonly believed that carbon only exists in the forms of diamond and graphite. In 1985, the discovery of fullerene by Kroto and coworkers (Kroto *et al.*, 1985) has changed the perception of scientists that very small dimension of carbon or perhaps a new carbon allotrope could be synthesized in a laboratory. This discovery has since stimulated researchers to study carbon of very small dimension more seriously. The real breakthrough on CNTs research came with Iijima's report of experimental observation of CNTs using transmission electron microscope (TEM) in 1991 (Iijima, 1991).

#### **1.4 Carbon Nanotubes**

CNTs have been called the most innovative materials of the 21<sup>st</sup> century due to their extraordinary properties and their enormous potential applications. Perhaps, CNTs are the most interesting carbon allotrope with large application potential. The structure of a nanotube is similar to that of graphite, which is like a cylinder of rolled graphene sheet with its body contains hexagonal rings and end cap with certain number of pentagonal rings. The end cap and body each has a structure similar to that of fullerene and graphite, respectively (Figure 1.4). Therefore, CNTs are also referred to at times as a hybrid structure of fullerene and graphite.



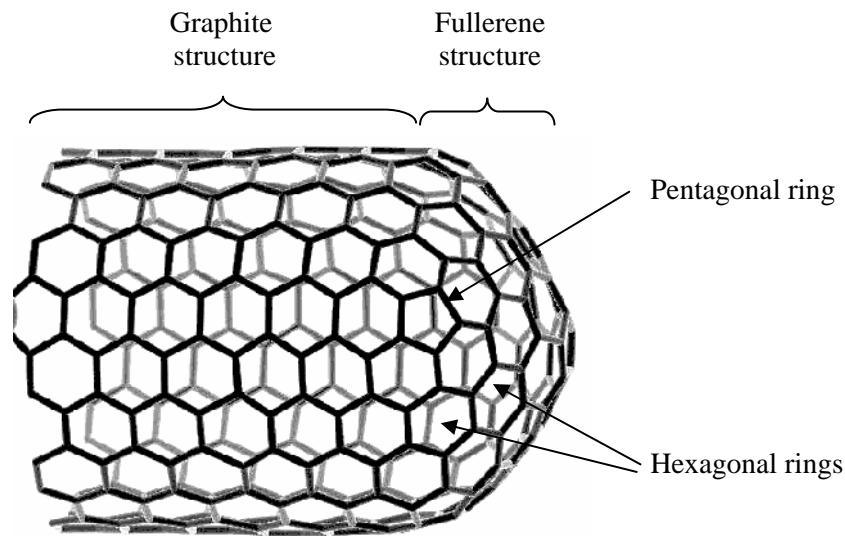


**Figure 1.4.** The structure of CNT with enclosed tip (Nanodimension, 2005).

CNTs can be categorized into two major groups based on the number of graphene sheets that forms their walls. A nanotube consisting of a single graphene sheet is referred to as single-walled CNT (SWNT). The nanotube that consists of two or more graphene sheets is named multi-walled CNT (MWNT). MWNT has an interlayer spacing of 0.34 – 0.36 nm, that is close to the typical atomic spacing of graphite, which is 0.335 nm. The C-C bonds that building up of CNTs have a length of 0.14 nm, which are shorter than the bonds in diamond. This indicates that CNTs are stronger than diamond (Bonard *et al.*, 2001). The diagram shown in Figure 1.5 represents: (a) a model of SWNTs bundle and (b) a model of MWNT with five graphene sheets. SWNTs are less stable as to stand alone due to their ultra-small size. Thus, most of the observed SWNTs appear in the bundle form, where the SWNTs are held by the weak *van der Waals* force.

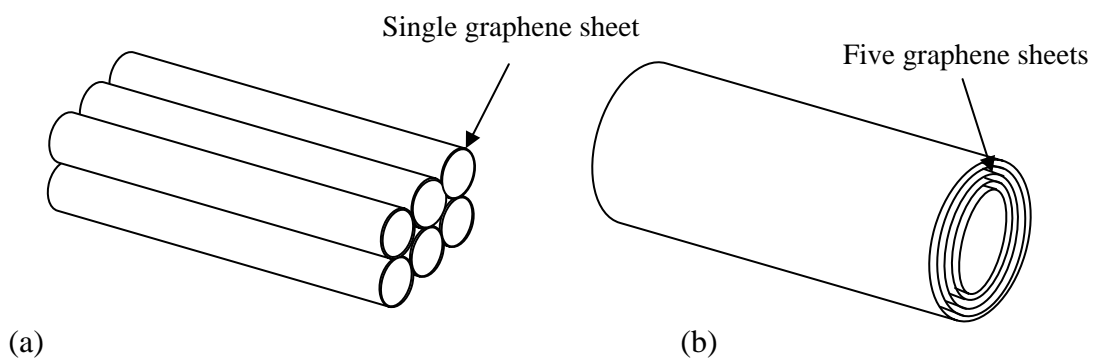


**Figure 1.5.** Schematic diagrams for (a) SWNTs in bundle form and (b) MWNT with five graphene sheets.

It is important to differentiate the following terms i.e. “filamentous carbons”, “carbon nanotubes (CNTs)” and “carbon nanofibers (CNFs)”. “Filamentous carbons” is a general term used to represent all carbon nanostructures with needle-like morphology. Filamentous carbons can be classified into two main categories on the basis of their structures, i.e. CNTs and CNFs. The nomenclature of CNTs and CNFs is ambiguous as no standardization on the terms used has been implemented so far. According to Vander Wal *et al.* (2001), CNTs are referred to as a highly graphitic structure with the orientation of the basal carbon planes parallel to the tube axis whereas CNFs are the structures with the other orientations of the graphitic lamella that will leave a smaller or no central channel (Figure 1.6). According to Pan *et al.* (2004) and Pérez-Cabero *et al.* (2003), the term “CNTs” is used to refer to the filamentous carbons with a significant center channel or hollow core. Filamentous carbons without or with insignificant central channel are denoted as “CNFs”, regardless of their graphitic structure (Figure 1.7). The terms used in this thesis for these carbon structures are defined according to those given by Pan *et al.* and Pérez-Cabero *et al.* as they are easily comprehended in explaining the types of filamentous carbons synthesized in the present study.

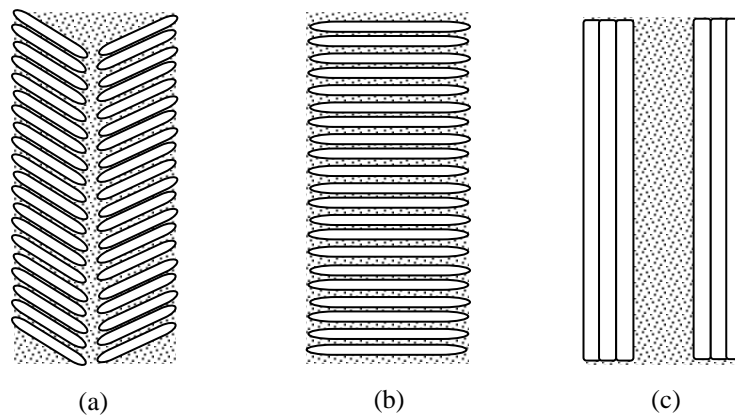


**Figure 1.6.** Schematic diagram presentation of the cross sections of (a,b) CNFs and (c) CNTs, with regard to their graphitic structures.

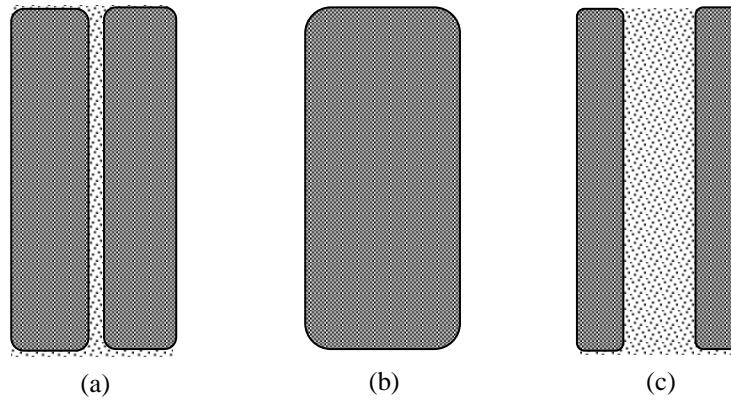


**Figure 1.7.** Schematic diagram presentation of the cross sections of (a,b) CNFs and (c) CNTs, with regardless to their graphitic structures.

## 1.5 Hydrogen

Hydrogen is an ultimate clean energy carrier. When it is combusted, heat and water are the only products. Therefore, the use of hydrogen as fuel can greatly reduce green house gas emissions. Moreover, development of affordable hydrogen fuel will help reducing our nation's dependence on oil, leading to an increased national energy security. Thus, hydrogen offers a potentially non-polluting, inexhaustible, efficient and cost attractive fuel for today's rising energy demands.

Future shortage of petroleum supply and surging prices of petroleum-based fuels, coupled with the increasing awareness of green house gas emissions increase the shift towards the alternative fuels sector. From Figure 1.8, it can be observed that over the decades hydrogen will increase its energy share dramatically, accounting for approximately 49% of the global final energy consumption by the end of the 21<sup>st</sup> century.

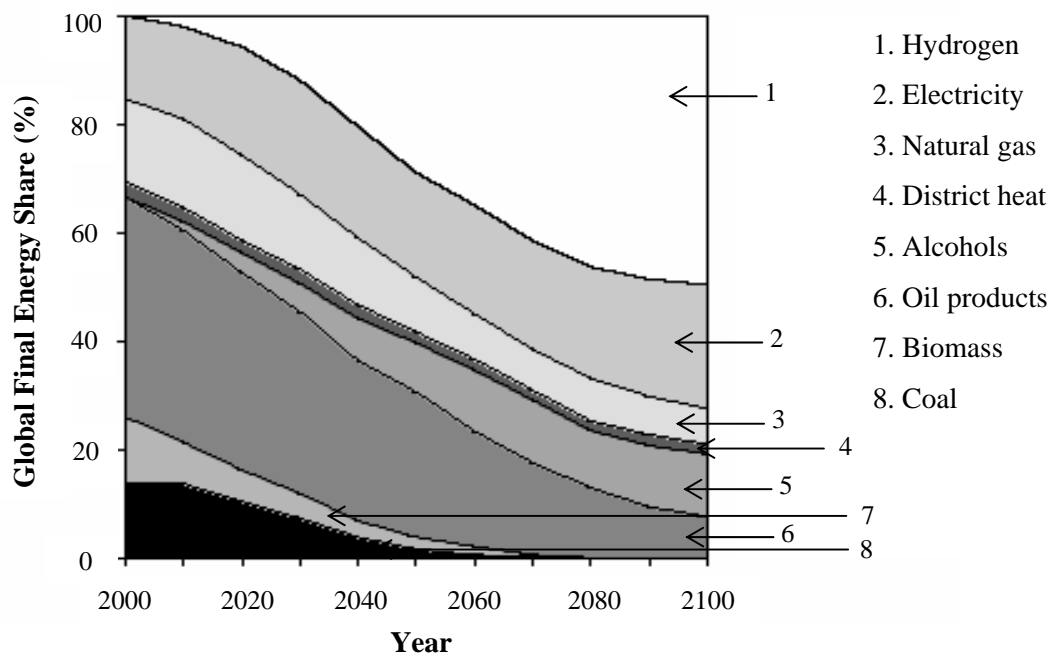


**Figure 1.8.** Evolution of global market shares of different energy carriers for the period 2000 – 2100. The alcohol category includes methanol and ethanol (Barreto *et al.*, 2003).

## 1.6 Natural Gas

Natural gas is a gaseous fossil fuel consisting primarily of methane and significant quantities of ethane, butane, propane, carbon dioxide, nitrogen, helium and hydrogen sulfide. Natural gas occurs in great abundance in some parts of the world, making a potential hydrocarbon feedstock and energy source that should not be underestimated. According to the recent Energy Information Administration (EIA)

report (EIA, 2007), Malaysia's natural gas reserve ranks 16<sup>th</sup> in the world with a total reserve of 75 trillion ft<sup>3</sup>. The total world's natural gas reserve records 6,183 trillion ft<sup>3</sup> in 2007. There will be a tremendous market for natural gas if more valued products can be obtained from it. Coupled with the current worldwide crude oil shortage, the role played by natural gas as a fuel and raw material is of increasing importance.

Table 1.1 shows the typical composition of natural gas and the composition of Malaysia natural gas. The composition of natural gas falls in a range for each of its component as the composition of natural gas from different reservoirs worldwide varies. Effective utilization of natural gas remains a challenge from the economic point of view. Natural gas itself can serve as fuel. However, for diversity, various routes have been considered for its conversion to value-added products, such as higher hydrocarbons, hydrogen and recently CNTs. Since methane is the major component of natural gas (70 – 90%), conversion of natural gas is always expressed scientifically as methane conversion.

**Table 1.1.** Composition of natural gas (NaturalGas, 2007; GasMalaysia, 2008).

<b>Components</b>		<b>Typical</b>	<b>Malaysia</b>
Methane	CH <sub>4</sub>	70-90%	92.73%
Ethane	C <sub>2</sub> H <sub>6</sub>		4.07%
Propane	C <sub>3</sub> H <sub>8</sub>	0-20%	0.77%
Butane	C <sub>4</sub> H <sub>10</sub>		0.14%
Carbon Dioxide	CO <sub>2</sub>	0-8%	1.83%
Oxygen	O <sub>2</sub>	0-0.2%	N.A.
Nitrogen	N <sub>2</sub>	0-5%	0.45%
Hydrogen sulphide	H <sub>2</sub> S	0-5%	N.A.
Rare gases	Ar, He, Ne, Xe	trace	N.A.
Other hydrocarbon		N.A.	0.01

## 1.7 Methane Activation

Figure 1.9 shows various paths of methane activation to other value-added products. Keller and Bhasin (1982) were the first to report the direct conversion of methane to ethylene. Following their work, oxidative coupling of methane (OCM) became one of the most pursued topics of research in methane activation. This is because hydrocarbon production via synthesis gas (syngas) is expensive and rather circuitous, and OCM prepares a simpler and cheaper route for the production of higher hydrocarbon from natural gas, using intermediate product, ethylene, as feedstock. Another process, known as steam reforming of methane (SRM), can be used for syngas production. Owing to SRM produces higher H<sub>2</sub> to CO ratio, being 3:1 (Figure 1.9), this process is widely applied in the gas industry for producing hydrogen on a large scale. Another alternative way to make syngas from methane is through partial oxidation of methane (POM). This reaction produces H<sub>2</sub> and CO in the ratio of 2:1. Carbon dioxide reforming of methane (CO<sub>2</sub>RM) is another way to produce syngas. This process produces H<sub>2</sub> and CO in the ratio of 1:1. It is noteworthy that the ratios of 2:1 and 1:1 are desirable H<sub>2</sub> to CO ratio for the downstream process. The syngas produced from the mentioned routes can be further converted into methanol, an important feedstock for the methanol to gasoline (MTG) process meant for producing gasoline (Chang, 1998). Alternatively, syngas can be directly processed into hydrocarbons via the Fischer-Tropsch (FT) process (Vannice, 1976).

Direct decomposition of methane has been proposed as an economical process to produce hydrogen. Unlike SRM, POM and CO<sub>2</sub>RM, methane decomposition process produces only H<sub>2</sub> and solid carbon, thereby eliminating the necessity for separation of CO<sub>x</sub> from H<sub>2</sub> product. The carbon product produced from methane decomposition has an additional advantage as various valuable types of

carbon, including carbon black, CNFs and CNTs, can be obtained as by-products from this process.

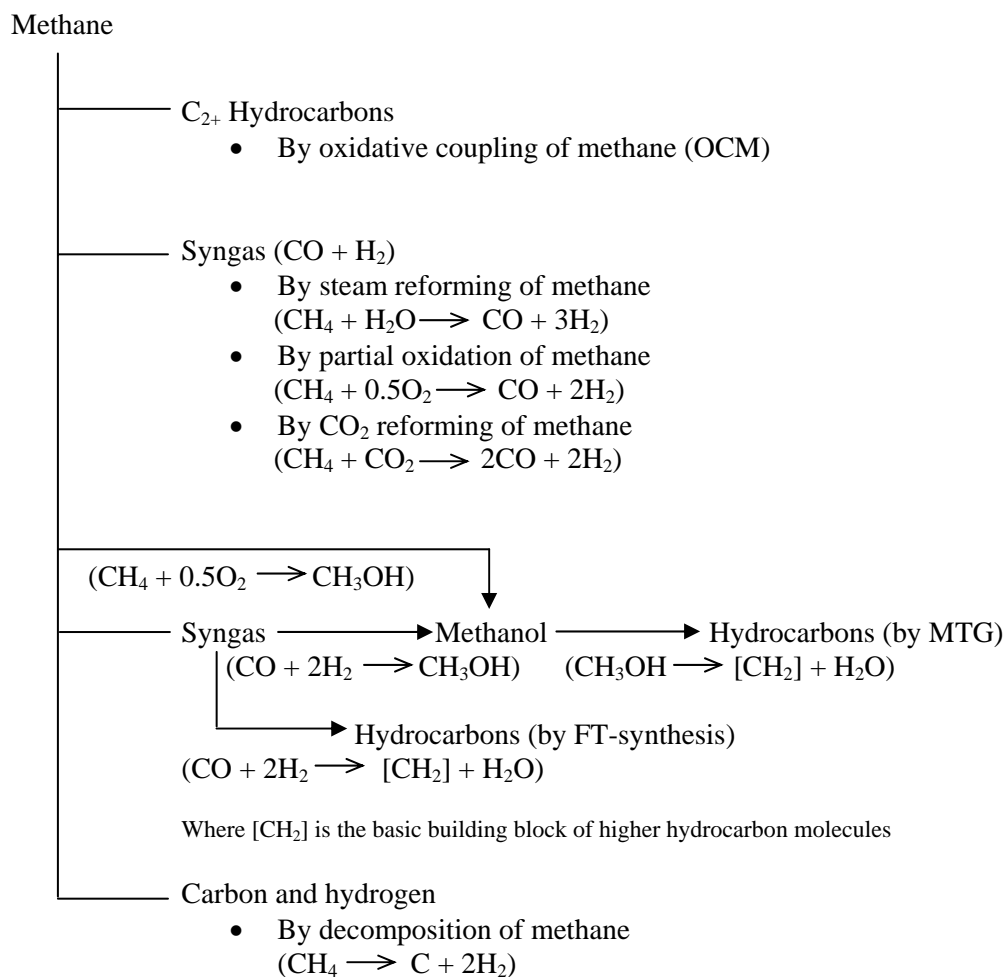


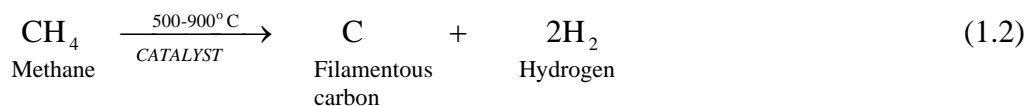
**Figure 1.9.** Various paths of methane activation to more value-added products (Choudhary *et al.*, 2003).

## 1.8 Methane Decomposition

Decomposition of methane can be categorized into two major types, representing thermal decomposition and catalytic decomposition. Thermal decomposition of methane (TDM) (equation 1.1) occurs at elevated temperatures, above 1200°C, in a thermal reactor without the presence of a catalyst (Shpilrain *et al.*, 1999; Muradov, 2001). This process produces hydrogen as the major product and clean carbon black as by-product. Carbon black is an important feedstock for rubber industry (Zuev and Michailov, 1970).



The reasons for not employing catalyst in the decomposition of methane is mainly due to the carbon formation will deactivate the catalyst and thus, decreasing the hydrogen yield. However, the TDM process is not economical for commercial hydrogen production as it requires very high operating temperatures. To overcome this drawback, specially designed catalyst is used, and it allows reducing the reaction temperature of the decomposition process. Methane decomposition with the presence of catalyst is widely known as catalytic decomposition of methane (CDM) (equation 1.2).



The types of catalysts used and the reaction conditions employed are the two important factors to be considered for a CDM process. Transition metals, especially



metals from group VIII (Fe, Co and Ni) in the periodic table, are normally used as catalytic materials. (Bethune *et al.*, 1993; Fan *et al.*, 1999; Takenaka *et al.*, 2003b; Zein *et al.*, 2006). The typical reaction temperatures for CDM are in a range of 500 - 900°C, a temperature which is much lower than that required by the TDM process. As a consequence of this, more attentions are focused on the CDM process by industrialist, researchers, scientists, etc. Also, not only hydrogen gas is produced, filamentous carbons can be produced as one of the valued products from the CDM process (Figure 1.10). It should be noted that filamentous carbons are more valuable than carbon black due to their excellent properties and their many promising applications. By proper designing of a catalyst and performing the CDM process at suitable reaction conditions, one can tailor-make the specific types of filamentous carbons for the needs of the market and this is one of the major researches that has attracted the great interest of many researchers around the world.

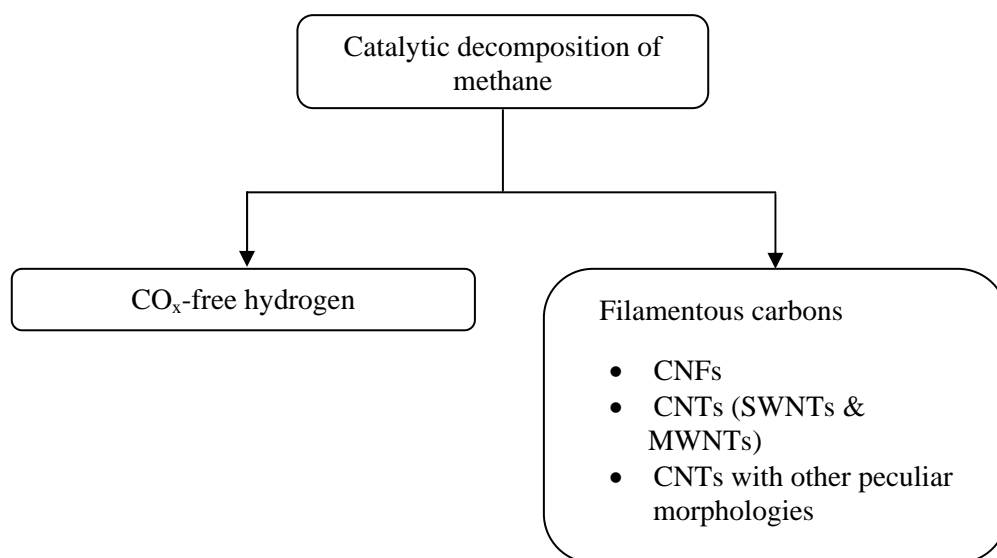


**Figure 1.10.** Flowchart showing the possible products obtained from CDM process.

## 1.9 Problem Statement

The discovery of CNTs using various technologies in the past 17 years has witnessed significant progress in their synthesis and applications. Even though CNTs have been successfully synthesized via various approaches, there are still technical challenges that must be investigated and overcome. To date, no one has successfully achieved controlled synthesis and cost effectively growing CNTs on a large scale. Controlled synthesis means one can tailor-make CNTs with the desirable structures and morphologies, such as MWNTs, SWNTs, Y-junction, specific diameter, etc., through designing the catalyst and optimizing the process conditions. Production of cost effectively growing CNTs can only be achieved when one can grow CNTs in high selectivity to the desired structures and morphologies at high yield and with minimum cost. Since CNTs are very new materials, the problems arising especially in their synthesis part need further investigation and research.

As most commonly known, electric arc-discharge (EAD), laser ablation (LA) and chemical vapor deposition (CVD) are prominent methods for CNTs synthesis. The said methods have both advantages and disadvantages. As an example, EAD and LA methods, which require very high temperature ( $\geq 3000$  °C), are not economical for scaling up the production of CNTs although both are efficient in producing SWNTs and MWNTs with fewer defects (Dai, 2001). CVD has been appreciated as the most promising method for producing CNTs on a large scale. Unfortunately, the CNTs produced by the said method are usually MWNTs and often riddled with defects.

CNTs of high quality and uniform diameter are essential to put the potential applications of CNTs into practice. This is attributable to the properties of CNTs: their metallic, semiconducting and mechanical properties depend strongly on their

diameter (Saito *et al.*, 1992; Odom *et al.*, 1998; Reich *et al.*, 2004). To date, many groups of researchers have successfully produced CNTs of good quality and nearly uniform diameters (Nikolaev *et al.*, 1999; Cheung *et al.*, 2002; Huh *et al.*, 2005; Kumar and Ando, 2005; Ren *et al.*, 2006). However, most of them involved with complicated catalyst preparation procedures and sophisticated equipment that resulted in rising catalyst and production costs. In addition, the CVD method favors very high reaction temperatures (900 – 1200°C) for producing SWNTs (Hu *et al.*, 2003; Liu *et al.*, 2003; Ando *et al.*, 2004). This is a major shortcoming as higher reaction temperature increases the cost of production as well as enhances the deposition of undesirable carbonaceous materials resulted from thermal-pyrolysis of methane. Furthermore, synthesizing SWNTs at a lower reaction temperature such as at 700°C is very difficult and truly a challenge. Therefore, it is necessary to develop a method that can produce various types of CNTs with the capability in controlling their growth to the desired structures, morphologies and uniformity at a lower temperature.

It cannot be denied that process and kinetic studies are also essential for successful design and application of CVD in producing CNTs. Unfortunately, the information pertaining to these studies is very limited in the literature. In addition, the growth mechanism of CNTs is still controversial. Therefore, it is imperative to conduct the process and the kinetic studies for investigating various process parameters that may influence and affect the yield and the growth mechanism of CNTs. The vital parts of the present work are to search and study the criteria for growing CNTs and achieving the controlled production by means of a simpler and cheaper approach.

## 1.10 Objectives

The present study has the following objectives:

- 1) To study the effects of catalyst components, including active metal, promoter and support, the effect of active metal to promoter ratio as well as the effect of metal amount loading, on methane decomposition into CNTs and CO<sub>x</sub>-free hydrogen.
- 2) To develop a relationship for the catalytic activity, the morphology of the produced CNTs and the CNTs growth mechanism with the nature of the catalyst used by performing various focal characterizations on both produced CNTs and developed catalysts.
- 3) To examine the effects of catalyst preparations, including the effect of catalyst calcination temperature, the effect of catalyst preparation methods, the effect of metal amount loading and the effect of catalyst reduction temperature on carbon yield and morphology of produced CNTs.
- 4) To evaluate the catalytic performance of the best catalyst in various process parameters, including reaction temperature, partial pressure of methane and catalyst weight. This is followed by analyzing, modeling and optimizing this process with respect to the simultaneous effects of these three process parameters on carbon yield and morphology of produced CNTs.
- 5) To perform kinetic study, including the determination of reaction rate, reaction order, rate constant and activation energy as well as rate-determining step (RDS) of methane decomposition over the best catalyst developed in this work.

### 1.11 Scope of the Study

The present study mainly focuses on catalyst development, process analysis as well as kinetic study for CNTs and CO<sub>x</sub>-free hydrogen production via CDM process. Catalytic activity test of the developed catalysts is carried out at atmospheric pressure in a vertical fixed-bed micro-reactor. The product gases are analyzed using an online gas chromatography (GC). The freshly prepared catalysts and used catalysts are characterized using surface area analyzer, scanning electron microscope (SEM), transmission electron microscope (TEM), thermal gravimetric analyzer (TGA), temperature-programmed reduction (TPR) apparatus, X-ray diffractometer (XRD) and Raman spectroscopy.

The aim of the catalyst development is to identify the most suitable supported catalysts used in the CDM that exhibit higher activity, selectivity and stability. In this regard, various active metals, promoters and catalyst supports are tested for CDM into CNTs and hydrogen. In this study, the selection of the active metals and promoters is limited to those only from Groups VIB, VIIB, VIII and IB in Row 4; and from Groups VIB and IB in Row 5 of the periodic table, respectively. These metals are chosen because they belong to the same group of metals, which are either active or effective as promoter for a catalyst in the CDM process. Noble metals that are in the same groups as those aforementioned metals are not considered in this study. This is because the non-noble metals are preferred commercially over noble metals, owing to the inherent availability and low costs of the former. The selection of catalyst supports covers Al<sub>2</sub>O<sub>3</sub>, MgO, CeO<sub>2</sub>, TiO<sub>2</sub>, La<sub>2</sub>O<sub>3</sub>, SiO<sub>2</sub> (Cab-osil) and zeolites. These supports are chosen because they are widely reported in the literature as promising catalyst supports used in many chemical reactions, especially in the

CDM reaction. It is essential to choose the most suitable support which compatible with the metal used and the reaction condition employed in this study.

Besides monometallic catalysts, bimetallic and trimetallic catalysts are also developed and tested in the present study. It is expected that addition of second and third metals component, such as CuO, CoO<sub>x</sub>, FeO<sub>x</sub>, MnO<sub>x</sub>, MoO<sub>x</sub>, NiO and etc., will further improve the overall performance of the catalysts. The suitability of the final developed catalyst in the CDM will be demonstrated. The effect of these catalyst components, namely active metals, promoters and catalyst supports on CNTs formation are also examined. In this regard, the yield and the morphology of the produced CNTs are characterized using surface area analyzer, Raman spectroscopy, SEM, TGA, TEM and XRD. The relationship between the catalytic activity and the morphologies of the produced CNTs with the nature of the catalyst material is developed. The possible growth mechanism for those structures with respect to the catalyst used is proposed.

In the process analysis, the effects of reaction temperature, partial pressure of methane and catalyst weight on methane decomposition are investigated using COST (change one separate factor at a time) approach. These factors are selected because they are reported to have influence either on the carbon yield or on the morphology of the produced CNTs. Data analysis is further studied using factorial design of response surface methodology (RSM) approach as to analyze the influences of each process variable and their interaction effects on carbon yield. This is followed by the determination of the optimum reaction condition from the set of experimental data collected. Lastly, kinetic study is carried out to obtain the reaction rate, reaction order, rate constant, activation energy and rate-determining step (RDS) of methane decomposition over the best catalyst developed in this work.

## **1.12 Organization of the Thesis**

This thesis consists of six chapters. Chapter 1 (Introduction) provides a brief description of catalysis, nanotechnology, allotropes of carbon, carbon nanotubes, hydrogen, natural gas as well as catalytic decomposition of methane process. This chapter also includes the problem statement that provides some basis and rationale to identify the research directions and objectives. The objectives and scopes of the study are then elucidated. This is followed by the organization of the thesis.

Chapter 2 (Literature Review) summarizes the past research works in the fields related to CNTs, including the properties and the potential applications of CNTs as well as their synthesis approaches. Synthesizing CNTs via CDM over supported catalysts is then being highlighted in this chapter. Possible growth mechanism of CNTs on supported catalysts is also reviewed and discussed. This serves as the background information about the specific problems that have to be addressed in this research work.

Chapter 3 (Materials and Methods) presents the details of the materials and chemicals used and the research methodology conducted in the present study. Detailed experimental setup is elaborated and shown in this chapter. This is followed by the discussion on the detailed experimental procedures, including catalyst preparations, CNTs synthesis procedures, process conditions and kinetic study. Finally, the analytical techniques and the conditions set for the equipment used for various characterizations of both CNTs and catalysts are presented.

Chapter 4 (Results and Discussion) presents and discusses all important findings obtained in this study. This chapter is the main part of the thesis and it comprises of six main sections based on the present experimental work. The main topics in this chapter include preliminary study on CDM process, CDM over

supported-nickel and -cobalt catalysts, effect of catalyst preparation, process analysis and kinetic study.

Chapter 5 (Conclusions) summarizes the results reported in the previous chapters and some concluding remarks are also made. The conclusions are obtained from each individual study carried out in the present research.

Chapter 6 (Recommendations) suggests the ways to improve the present studies and recommend the possible future studies in this field. These recommendations and suggestions are given after taking into consideration the significant findings, the conclusions obtained as well as the limitations and difficulties encountered in the present work.



## CHAPTER 2

### LITERATURE REVIEW

#### 2.1 Carbon Nanotubes

##### 2.1.1 History of filamentous carbons

The history of filamentous carbons goes back to more than a century. The first filamentous carbons were synthesized by Thomas A. Edison in the 19<sup>th</sup> century to be used in an electric bulb (Dresselhaus and Endo, 2001). However, the study on filamentous carbons after Edison proceeded slowly due to the fact that most of the filamentous carbons had been replaced by more sturdy tungsten filaments. In 1975, Endo had reported the synthesis of carbon nanofilaments through catalyzed cracking of hydrocarbons in his PhD thesis (Endo, 1975; Dresselhaus and Avouris, 2001; Dresselhaus and Endo, 2001). At almost the same time, Obelin and coworkers reported carbon filaments of very small diameter (less than 10 nm) had been produced from decomposition of benzene at high temperatures (Oberlin *et al.*, 1976a; Oberlin *et al.*, 1976b). However, the studies of such very thin filaments were not systematically reported in those early years due to the limitation of the characterization equipment. The real breakthrough in the studies of carbon nanostructures was in 1985 when fullerenes were discovered by Kroto, Curl and Smalley (Kroto *et al.*, 1985). This discovery since then had stimulated the systematical study on the very small diameter carbon structures.

It is widely known that fullerene is a zero-dimensional carbon allotrope, whereas graphite and diamond are generally considered as two- and three-dimensional structures, respectively. For this reason, scientists predicted that carbon allotrope of one-dimensional structure should be stable enough to exist

independently. In 1991, this speculation became a reality when the one-dimensional carbon structure was first discovered by a Japanese microscopist, Sumio Iijima (Iijima, 1991) in the Nippon Electric Company (NEC) Laboratory in Tsukuba, Japan. Under the transmission electron microscope (TEM) observation, this carbon structure appeared in the form of thread with significant hollow center core. Owing to its emplacement on the nano-scale and its thread-like structure, this carbon structure was named “carbon nanotubes (CNTs)”. Nowadays, CNTs are universally accepted as the fourth carbon allotrope. Figure 2.1 shows the structures of carbon allotropes including graphite, diamond, fullerene and CNTs. The first CNTs observed by Iijima were multi-wall carbon nanotubes (MWNTs). In 1993, single-walled carbon nanotubes (SWNTs) were discovered at almost the same time by Iijima and coworkers (Iijima and Ichihashi, 1993) in the NEC laboratory and by Bethune and coworkers (Bethune *et al.*, 1993) in the IBM Almaden laboratory.

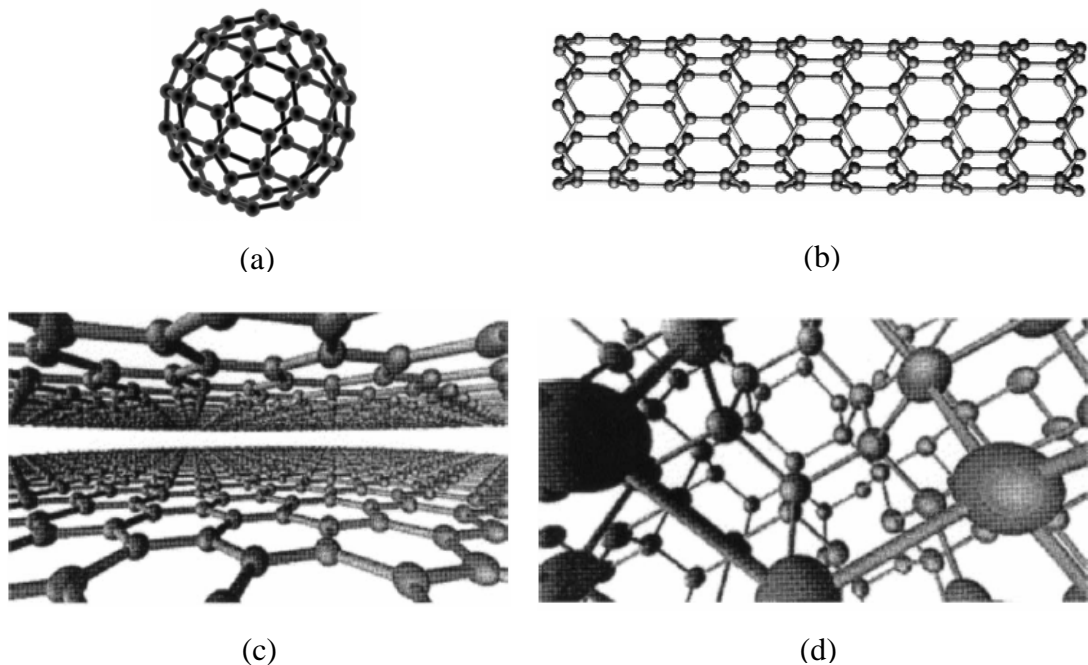


**Figure 2.1.** The different structures of carbon allotropes: (a) fullerene (0-D), (b) carbon nanotubes (1-D), (c) graphite (2-D) and (d) diamond (3-D) (Cohen, 2001).

### 2.1.2 Structure of carbon nanotubes

To have a basic understanding of the structure of CNTs is to visualize the folding of a graphene sheet into a tube. The folding can be done in many different angles to form armchair, zigzag or chiral nanotubes. Referring to Figure 2.2, the chiral vector  $C_h$  is defined as a line connecting two crystallographically equivalent sites  $O$  and  $C$  on a two-dimensional graphene structure. The chiral vector can be defined in terms of the lattice translation indices  $(n, m)$  (Dresselhaus *et al.*, 1992). The chiral angle ( $\theta$ ) is an angle measured between the chiral vector  $C_h$  with respect to the zigzag direction  $(n, 0)$ . The armchair nanotube is defined as  $\theta = 30^\circ$  and the translation indices is  $(n, n)$ . A general  $\theta$  direction, with  $0 < \theta < 30^\circ$ , gives the formation of chiral  $(n, m)$  nanotubes. The structures of zigzag, armchair and chiral nanotube are shown in Figure 2.3.

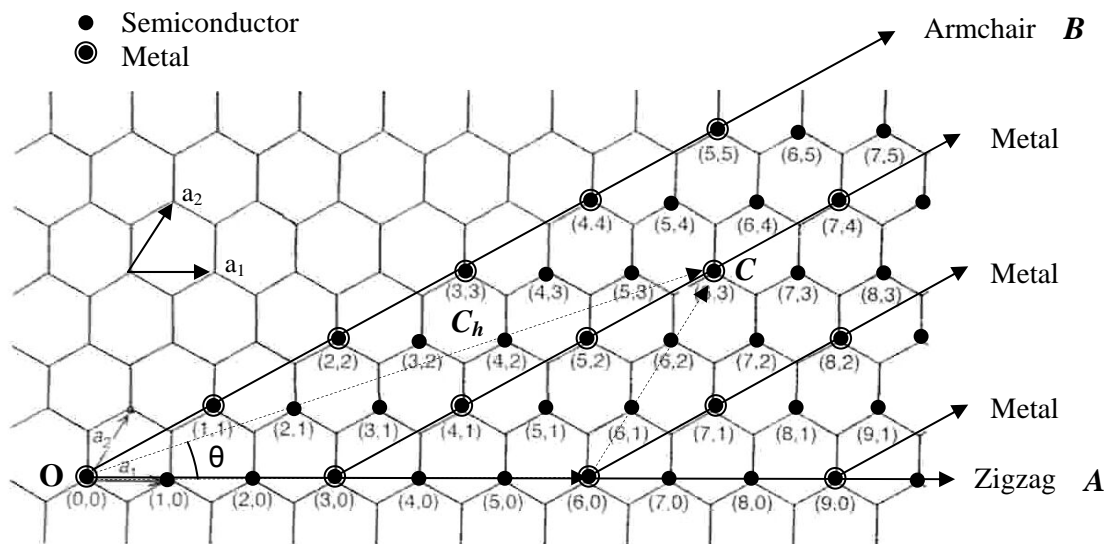


**Figure 2.2.** The two-dimensional graphene sheet given chiralities  $(n, m)$  (Dresselhaus and Avouris, 2001).